Electronic Supplementary Information

for

Diastereomeric dinickel(II) complexes with non-innocent bis(octaazamacrocyclic) ligands: isomerization, spectroelectrochemistry, DFT calculations and use in catalytic oxidation of cyclohexane

Anatolie Dobrov,[†,Δ] Denisa Darvasiová,[#] Michal Zalibera,[#,*] Lukáš Bučinský,[#] Ingrid Jelemenská,[#,◊] Peter Rapta,[#] Sergiu Shova,[‡] Dan G. Dumitrescu,[♦] Marta A. Andrade,[§] Luísa M. D. R. S. Martins,[§,*] Armando J. L. Pombeiro,[§,&] Vladimir B. Arion[†,*]

[†]*University of Vienna, Institute of Inorganic Chemistry, Währinger Strasse 42, A-1090 Vienna, Austria*

[Δ]*Universität Wien, Fakultät für Chemie, Institut für Biophysikalische Chemie, 1090 Wien, Austria*

[#]*Institute of Physical Chemistry and Chemical Physics, Faculty of Chemical and Food Technology, Slovak University of Technology in Bratislava, Radlinského 9, SK-81237 Bratislava, Slovak Republic*

[◊]*Department of Chemistry, Faculty of Natural Sciences, Constantine the Philosopher University in Nitra, 949 74 Nitra, Slovak Republic*

[‡]*Inorganic Polymers Department, "Petru Poni" Institute of Macromolecular Chemistry, Aleea Gr. Ghica Voda 41 A, Iasi 700487, Romania*

[♦]*Elettra - Sincrotrone Trieste S.C.p.A., Strada Statale 14 - km 163,5 in AREA Science Park 34149 Basovizza, Trieste, Italy*

[§]*Centro de Química Estrutural, Institute of Molecular Sciences, Universidade de Lisboa, Av. Rovisco Pais, 1049-001 Lisboa, Portugal*

[&]*Peoples' Friendship University of Russia (RUDN University), Research Institute of Chemistry, 6 Miklukho-Maklaya Street, Moscow 117198, Russian Federation*

Table of Contents
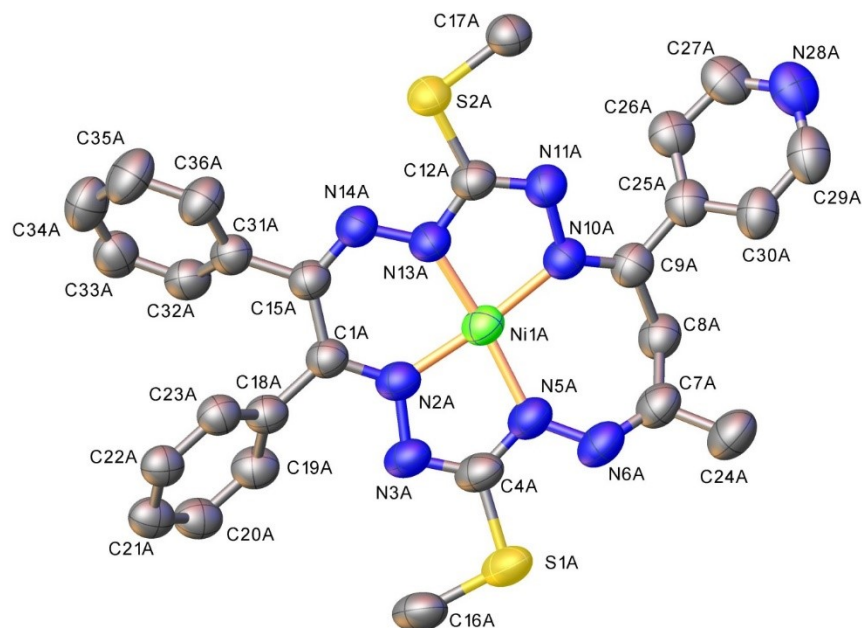
Crystallography

Figure S1. View of the asymmetric unit in the crystal structure of **5s** with atom labelling and thermal ellipsoids at 40% probability level. Only a half-moiety of dimeric complex (denoted as **A** part) is shown. Co-crystallized molecules of ethanol are not shown.
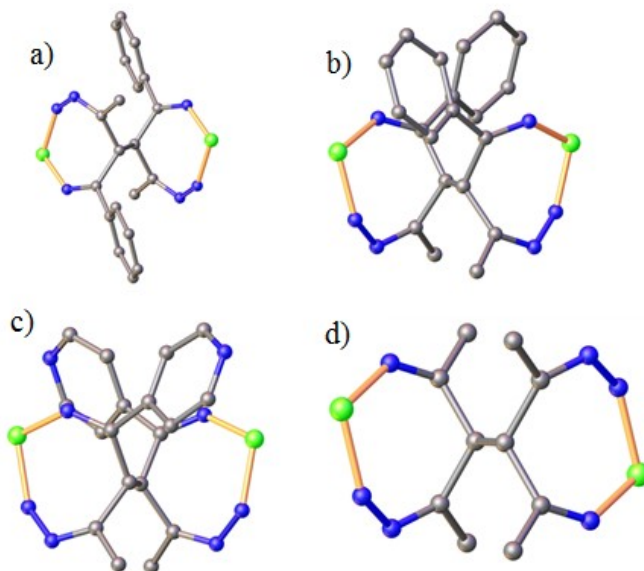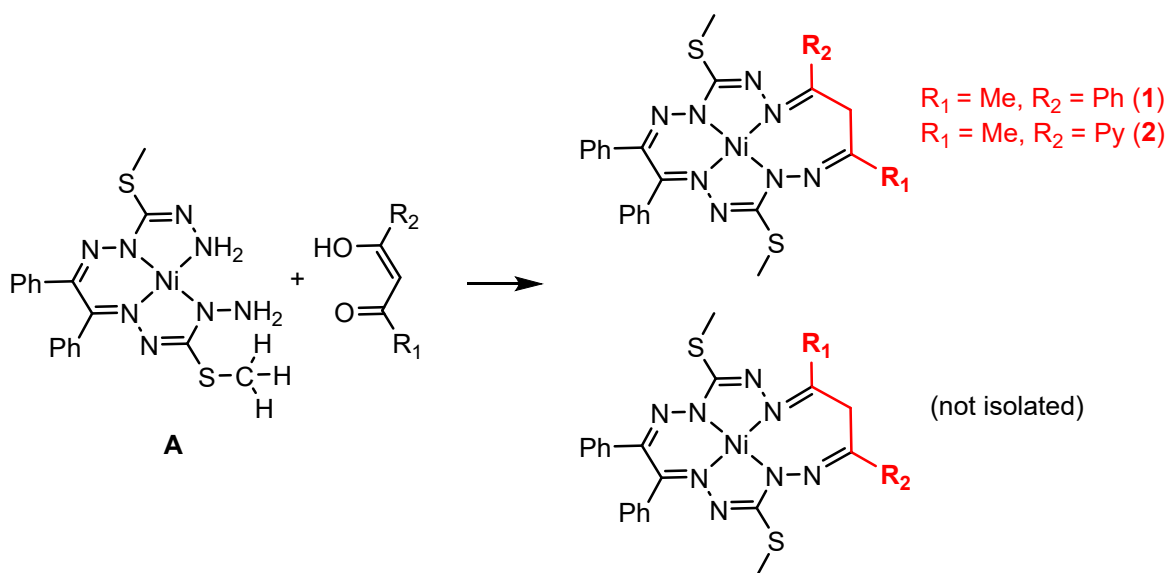

Figure S2. Relative arrangements of Ph, Me and Py substituents and N–N backbones at/in 7-membered chelate rings in a) **4a** (*S,R*) b) **4s** (*S,S*) c) **5s** (*R,R*) and d) **6a** (*S,R*).

R$_1$ = Me, R$_2$ = Ph (**1**)
R$_1$ = Me, R$_2$ = Py (**2**)

(not isolated)

A

Scheme S1. Synthesis of **1**–**2**. Expected products on the bottom have not been isolated.

Table S1. Bond distances (Å) and angles (°).

Compound **4a**

Distances	exp.	DFT	Distances	exp.	DFT
Ni1-N2	1.832(3)	1.864	C7-C24	1.511(5)	1.508
Ni1-N5	1.864(3)	1.891	C8-C8[1]	1.573(6)	1.583
Ni1-N10	1.889(3)	1.912	C8-C9	1.518(4)	1.527
Ni1-N13	1.809(3)	1.832	C9-C25	1.476(4)	1.490
S1-C4	1.747(3)	1.773	C15-C31	1.499(5)	1.496
S1-C16	1.801(4)	1.827	C18-C19	1.381(5)	1.400
S2-C12	1.736(3)	1.764	C18-C23	1.393(5)	1.398
S2-C17	1.803(3)	1.826	C19-C20	1.384(5)	1.392
N2-N3	1.391(4)	1.375	C20-C21	1.390(5)	1.396
N2-C1	1.327(4)	1.319	C21-C22	1.377(5)	1.393
N3-C4	1.314(4)	1312	C22-C23	1.396(5)	1.394
N5-N6	1.390(4)	1.363	C25-C26	1.391(5)	1.401
N5-C4	1.358(4)	1.358	C25-C30	1.402(5)	1.402
N6-C7	1.283(4)	1.281	C26-C27	1.378(5)	1.391
N10-N11	1.426(4)	1.402	C27-C28	1.376(6)	1.394
N10-C9	1.310(4)	1.297	C28-C29	1.375(6)	1.393
N11-C12	1.294(4)	1.300	C29-C30	1.378(5)	1.392
N13-N14	1.338(4)	1.323	C31-C32	1.386(5)	1.401
N13-C12	1.381(4)	1.374	C31-C36	1.394(5)	1.401
N14-C15	1.315(4)	1.310	C32-C33	1.390(6)	1.393
C1-C15	1.445(5)	1.459	C33-C34	1.369(6)	1.394
C1-C18	1.488(5)	1.495	C34-C35	1.373(6)	1.395
C7-C8	1.513(5)	1.533	C35-C36	1.384(6	1.393

Angles	exp.	DFT
N2-Ni1-N5	83.52(12)	83.4
N2-Ni1-N10	173.73(12)	173.9

N5-Ni1-N10	102.55(12)	102.1
N13-Ni1-N2	91.77(12)	91.6
N13-Ni1-N5	171.46(13)	169.7
N13-Ni1-N10	82.40(12)	82.5
C4-S1-C16	99.59(17)	100.7
C12-S2-C17	99.79(16)	100.6
N3-N2-Ni1	116.3(2)	115.1
C1-N2-Ni1	128.8(2)	127.2
C1-N2-N3	114.8(3)	117.6
C4-N3-N2	108.8(3)	110.2
N6-N5-Ni1	137.2(2)	135.6
C4-N5-Ni1	110.1(2)	108.7
C4-N5-N6	111.2(3)	112.9
C7-N6-N5	119.3(3)	122.7
N11-N10-Ni1	114.4(2)	112.3
C9-N10-Ni1	131.1(2)	131.3
C9-N10-N11	114.5(3)	116.3
C12-N11-N10	108.1(3)	110.1
N14-N13-Ni1	132.6(2)	131.5
N14-N13-C12	114.1(3)	116.7
C12-N13-Ni1	113.3(2)	111.7
C15-N14-N13	119.4(3)	120.7
N2-C1-C15	120.4(3)	121.4
N2-C1-C18	118.8(3)	119.2
C15-C1-C18	120.7(3)	119.2
N3-C4-S1	119.0(3)	119.4
N3-C4-N5	120.7(3)	121.2
N5-C4-S1	120.3(3)	119.4
N6-C7-C8	128.0(3)	127.6
N6-C7-C24	116.1(3)	116.3

C24-C7-C8	115.8(3)	116.1
C7-C8-C8[1]	112.4(3)	112.7
C7-C8-C9	116.1(3	115.0

Symmetry code: [1] 1– *x*, 2–*y*, –*z*.

Compound 4s

Distances	exp.	DFT	Distances	exp.	DFT
C1A-N2A	1.322(2)	1.319	C20B-C21B	1.387(5)	1.393
C1A-C15A	1.455(3)	1.459	C21A-C22A	1.387(4)	1.396
C1A-C18A	1.494(3)	1.496	C21B-C22B	1.383(5)	1.396
C1B-N2B	1.326(3)	1.319	C22A-C23A	1.395(3)	1.392
C1B-C15B	1.458(3)	1.459	C22B-C23B	1.393(3)	1.392
C1B-C18B	1.495(3)	1.496	C25A-C26A	1.398(3)	1.403
C4A-N3A	1.316(2)	1.312	C25A-C30A	1.401(3)	1.402
C4A-N5A	1.351(2)	1.356	C25B-C30B	1.403(3)	1.403
C4A-S1A	1.752(2)	1.773	C25B-C26B	1.399(3)	1.391
`C4B-N3B	1.316(3)	1.312	C26A-C27A	1.391(3)	1.392
C4B-N5B	1.351(2)	1.356	C26B-C27B	1.387(3)	1.395
C4B-S1B	1.757(2)	1.773	C27A-C28A	1.391(4)	1.393
C7A-N6A	1.288(2)	1.281	C27B-C28B	1.392(4)	1.393
C7A-C24A	1.499(3)	1.506	C28A-C29A	1.384(4)	1.395
C7A-C8A	1.523(3)	1.533	C28B-C29B	1.391(4)	1.392
C7B-N6B	1.284(3)	1.281	C29A-C30A	1.397(3)	1.391
C7B-C24B	1.498(3)	1.506	C29B-C30B	1.393(3)	1.392
C7B-C8B	1.529(3)	1.533	C31A-C32A	1.391(3)	1.401
C8A-C9A	1.518(3)	1.527	C31A-C36A	1.393(3)	1.401
C8A-C8B	1.574(3)	1.584	C31B-C32B	1.397(3)	1.401
C8B-C9B	1.517(3)	1.527	C31B-C36B	1.402(3)	1.401
C9A-N10A	1.298(2)	1.297	C32A-C33A	1.398(3)	1.393
C9A-C25A	1.494(3)	1.492	C32B-C33B	1.397(3)	1.393

C9B-N10B	1.297(2)	1.298	C33A-C34A	1.384(3)	1.394
C9B-C25B	1.495(3)	1.491	C33B-C34B	1.383(3)	1.394
C12A-N11A	1.300(3)	1.300	C34A-C35A	1.386(3)	1.394
C12A-N13A	1.376(2)	1.373	C34B-C35B	1.387(3)	1.394
C12A-S2A	1.7485(19)	1.765	C35A-C36A	1.393(3)	1.393
C12B-N11B	1.303(3)	1.300	C35B-C36B	1.396(3)	1.393
C12B-N13B	1.381(2)	1.373	N2A-N3A	1.394(2)	1.376
C12B-S2B	1.747(2)	1.765	N2A-Ni1A	1.850(2)	1.867
C15A-N14A	1.314(3)	1.310	N2B-N3B	1.393(2)	1.376
C15A-C31A	1.496(3)	1.496	N2B-Ni1B	1.853(2)	1.866
C15B-N14B	1.315(3)	1.310	N5A-N6A	1.390(2)	1.369
C15B-C31B	1.498(3)	1.496	N5A-Ni1A	1.868(2)	1.889
C16A-S1A	1.803(2)	1.827	N5B-N6B	1.390(2)	1.369
C16B-S1B	1.810(2)	1.827	N5B-Ni1B	1.868(2)	1.888
C17A-S2A	1.806(2)	1.827	N10A-N11A	1.417(2)	1.402
C17B-S2B	1.805(2)	1.826	N10A-Ni1A	1.906(2)	1.919
C18A-C23A	1.396(3)	1.399	N10B-N11B	1.420(2)	1.401
C18A-C19A	1.400(3)	1.398	N10B-Ni1B	1.903(2)	1.920
C18B-C19B	1.396(3)	1.398	N13A-N14A	1.339(2)	1.323
C18B-C23B	1.398(3)	1.399	N13A-Ni1A	1.806(2)	1.831
C19A-C20A	1.388(3)	1.394	N13B-N14B	1.330(2)	1.323
C19B-C20B	1.390(3)	1.394	N13B-Ni1B	1.806(2)	1.831
C20A-C21A	1.386(4)	1.393			

Angles	exp.	DFT	Angles	exp.	DFT
N2A-C1A-C15A	120.71(17)	121.5	C29B-C28B-C27B	119.8(2)	119.6
N2A-C1A-C18A	119.31(17)	119.2	C28A-C29A-C30A	120.3(2)	120.1
C15A-C1A-C18A	119.98(16)	119.2	C28B-C29B-C30B	120.1(2)	120.4
N2B-C1B-C15B	120.78(17)	121.5	C29A-C30A-C25A	120.4(2)	120.8
N2B-C1B-C18B	118.31(18)	119.2	C29B-C30B-C25B	120.3(2)	120.6

C15B-C1B-C18B	119.98(16)	119.2	C32A-C31A-C36A	119.39(18)	118.5
N3A-C4A-N5A	121.20(17)	121.3	C32A-C31A-C15A	118.92(18)	121.6
N3A-C4A-S1A	121.20(17)	119.6	C36A-C31A-C15A	118.92(18)	119.8
N5A-C4A-S1A	119.96(14)	119.1	C32B-C31B-C36B	118.71(19)	118.5
N3B-C4B-N5B	118.81(14)	121.3	C32B-C31B-C15B	123.12(19)	121.6
N3B-C4B-S1B	121.21(17)	119.6	C36B-C31B-C15B	118.03(18)	119.8
N5B-C4B-S1B	119.66(15)	119.1	C31A-C32A-C33A	119.8(2)	120.8
N6A-C7A-C24A	117.00(17)	116.3	C33B-C32B-C31B	120.3(2)	120.8
N6A-C7A-C8A	127.38(17)	127.1	C34A-C33A-C32A	120.4(2)	120.2
C24A-C7A-C8A	115.57(16)	116.6	C34B-C33B-C32B	120.6(2)	120.2
N6B-C7B-C24B	116.70(17)	116.3	C33A-C34A-C35A	120.1(2)	119.5
N6B-C7B-C8B	127.12(17)	127.2	C35B-C34B-C33B	119.8(2)	119.5
C24B-C7B-C8B	116.09(17)	116.5	C34A-C35A-C36A	119.6(2)	120.3
C9A-C8A-C7A	115.20(15)	114.8	C34B-C35B-C36B	120.1(2)	120.3
C9A-C8A-C8B	114.44(15)	114.0	C35A-C36A-C31A	120.7(2)	120.7
C7A-C8A-C8B	110.23(15)	110.7	C35B-C36B-C31B	120.5(2)	120.7
C9B-C8B-C7B	116.24(16)	114.8	C1A-N2A-N3A	116.17(16)	117.4
C9B-C8B-C8A	113.48(15)	114.0	C1A-N2A-Ni1A	127.69(13)	127.2
C7B-C8B-C8A	109.66(15)	110.7	N3A-N2A-Ni1A	116.13(12)	115.2
N10A-C9A-C25A	124.55(17)	123.3	C1B-N2B-N3B	116.25(16)	117.5
N10A-C9A-C8A	120.03(16)	120.3	C1B-N2B-Ni1B	128.31(14)	127.2
C25A-C9A-C8A	115.35(16)	116.3	N3B-N2B-Ni1B	115.39(13)	115.3
N10B-C9B-C25B	123.62(17)	123.3	C4A-N3A-N2A	108.62(15)	110.1
N10B-C9B-C8B	120.66(17)	120.3	C4B-N3B-N2B	109.29(16)	110.1
C25B-C9B-C8B	115.65(16)	116.4	C4A-N5A-N6A	113.74(15)	113.4
N11A-C12A-N13A	120.29(17)	120.1	C4A-N5A-Ni1A	110.51(12)	109.2
N11A-C12A-S2A	122.69(15)	121.4	N6A-N5A-Ni1A	133.37(13)	133.9
N13A-C12A-S2A	117.01(14)	118.6	C4B-N5B-N6B	113.21(16)	113.5
N11B-C12B-N13B	119.89(18)	120.0	C4B-N5B-Ni1B	110.30(13)	109.2
N11B-C12B-S2B	122.78(15)	121.3	N6B-N5B-Ni1B	134.17(13)	133.6

N13B-C12B-S2B	117.32(15)	118.6	C7A-N6A-N5A	118.40(16)	121.7
N14A-C15A-C1A	126.28(17)	125.7	C7B-N6B-N5B	118.97(16)	121.6
N14A-C15A-C31A	112.52(16)	113.7	C9A-N10A-N11A	115.49(16)	116.2
C1A-C15A-C31A	120.99(17)	120.5	C9A-N10A-Ni1A	130.31(13)	131.3
N14B-C15B-C1B	125.58(18)	125.7	N11A-N10A-Ni1A	113.87(12)	112.5
N14B-C15B-C31B	111.15(17)	113.6	C9B-N10B-N11B	114.96(16)	116.2
C1B-C15B-C31B	111.15(17)	120.6	C9B-N10B-Ni1B	130.55(14)	131.3
C23A-C18A-C19A	119.12(19)	119.2	N11B-N10B-Ni1B	113.94(12)	112.4
C23A-C18A-C1A	122.30(18)	120.6	C12A-N11A-N10A	108.48(15)	110.2
C19A-C18A-C1A	118.57(18)	120.2	C12B-N11B-N10B	108.44(16)	110.2
C19B-C18B-C23B	119.3(2)	119.2	N14A-N13A-C12A	114.51(16)	116.5
C19B-C18B-C1B	119.9(2)	120.6	N14A-N13A-Ni1A	132.31(13)	131.6
C23B-C18B-C1B	120.8(2)	120.6	C12A-N13A-Ni1A	113.06(13)	111.8
C20A-C19A-C18A	120.5(2)	120.4	N14B-N13B-C12B	114.17(16)	116.5
C20B-C19B-C18B	120.1(3)	120.4	N14B-N13B-Ni1B	132.58(14)	131.6
C19A-C20A-C21A	120.0(2)	120.2	C12B-N13B-Ni1B	113.23(13)	111.8
C21B-C20B-C19B	120.3(3)	120.2	C15A-N14A-N13A	119.75(16)	120.8
C22A-C21A-C20A	120.1(2)	119.7	C15B-N14B-N13B	120.60(17)	120.8
C22B-C21B-C20B	119.9(2)	119.7	N13A-Ni1A-N2A	92.27(7)	91.9
C21A-C22A-C23A	120.2(2)	120.2	N13A-Ni1A-N5A	169.01(8)	169.8
C21B-C22B-C23B	120.4(3)	120.2	N2A-Ni1A-N5A	83.24(7)	83.3
C22A-C23A-C18A	120.0(2)	120.4	N13A-Ni1A-N10A	82.50(7)	82.6
C22B-C23B-C18B	120.0(3)	120.4	N2A-Ni1A-N10A	172.32(7)	174.5
C26A-C25A-C30A	118.72(18)	118.5	N5A-Ni1A-N10A	102.88(7)	102.2
C26A-C25A-C9A	121.83(18)	122.3	N13B-Ni1B-N2B	91.84(7)	91.9
C30A-C25A-C9A	119.22(17)	119.2	N13B-Ni1B-N5B	170.96(8)	169.8
C30B-C25B-C26B	119.15(19)	118.5	N2B-Ni1B-N5B	83.71(7)	83.3
C30B-C25B-C9B	119.61(18)	119.2	N13B-Ni1B-N10B	82.50(7)	82.6
C26B-C25B-C9B	121.07(18)	122.3	N2B-Ni1B-N10B	173.11(7)	174.4
C27A-C26A-C25A	120.5(2)	120.6	N5B-Ni1B-N10B	102.44(7)	102.3

C27B-C26B-C25B	120.2(2)	120.8	C4A-S1A-C16A	101.30(10)	100.9
C26A-C27A-C28A	120.3(2)	120.4	C4B-S1B-C16B	101.43(10)	100.8
C26B-C27B-C28B	120.3(2)	120.1	C12A-S2A-C17A	100.65(10)	100.7
C29A-C28A-C27A	119.7(2)	119.6	C12B-S2B-C17B	100.16(10)	100.6

Compound **5s**

Distances	exp.	DFT	Distances	exp.	DFT
C1A-C15A	1.449(5)	1.462	N2A-Ni1A	1.844(3)	1.864
C1A-C18A	1.484(5)	1.495	N5A-N6A	1.390(5)	1.370
C1A-N2A	1.333(5)	1.318	N5A-Ni1A	1.875(3)	1.893
C4A-N3A	1.305(5)	1.313	N10A-N11A	1.419(4)	1.399
C4A-N5A	1.355(5)	1.357	N10A-Ni1A	1.896(3)	1.917
C4A-S1A	1.752(4)	1.770	N13A-N14A	1.350(4)	1.326
C7A-C8A	1.512(6)	1.535	N13A-Ni1A	1.807(3)	1.831
C7A-C24A	1.499(6)	1.504	C1B-C15B	1.448(6)	1.462
C7A-N6A	1.293(6)	1.278	C1B-N2B	1.330(5)	1.318
C8A-C9A	1.523(5)	1.524	C4B-N3B	1.339(6)	1.313
C8A-C8B	1.570(5)	1.578	C4B-N5B	1.286(5)	1.357
C9A-C25A	1.488(5)	1.488	C4B-S1B	1.747(5)	1.770
C9A-N10A	1.293(5)	1.298	C7B-C8B	1.531(5)	1.535
C12A-N11A	1.311(5)	1.304	C7B-C24B	1.516(6)	1.504
C12A-N13A	1.373(4)	1.373	C7B-N6B	1.274(5)	1.280
C12A-S2A	1.738(3)	1.761	C8B-C9B	1.505(6)	1.524
C15A-C31A	1.492(5)	1.496	C9B-C25B	1.495(6)	1.489
C15A-N14A	1.311(4)	1.309	C9B-N10B	1.283(5)	1.298
C16A-S1A	1.784(5)	1.827	C12B-N11B	1.312(5)	1.304
C17A-S2A	1.796(4)	1.827	C12B-N13B	1.389(5)	1.373
C18A-C19A	1.405(5)	1.398	C12B-S2B	1.728(4)	1.761
C18A-C23A	1.387(5)	1.399	C15B-N14B	1.290(5)	1.309
C19A-C20A	1.383(6)	1.394	C16B-S1B	1.799(6)	1.827

C20A-C21A	1.373(6)	1.393	C17B-S2B	1.789(5)	1.827
C21A-C22A	1.377(5)	1.396	C25B-C26B	1.388(6)	1.397
C22A-C23A	1.381(5)	1.391	C25B-C30B	1.372(6)	1.401
C25A-C26A	1.393(6)	1.397	C26B-C27B	1.380(6)	1.393
C25A-C30A	1.388(6)	1.401	C27B-N28B	1.307(6)	1.336
C26A-C27A	1.374(6)	1.393	C29B-C30B	1.389(7)	1.389
C27A-N28A	1.331(6)	1.336	C29B-N28B	1.346(6)	1.340
C29A-C30A	1.400(6)	1.389	N2B-N3B	1.393(5)	1.375
C29A-N28A	1.331(6)	1.340	N2B-Ni1B	1.839(3)	1.864
C31A-C32A	1.373(5)	1.401	N5B-N6B	1.396(5)	1.370
C31A-C36A	1.387(5)	1.401	N5B-Ni1B	1.882(4)	1.862
C32A-C33A	1.396(6)	1.393	N10B-N11B	1.423(4)	1.400
C33A-C34A	1.355(7)	1.394	N10B-Ni1B	1.892(3)	1.917
C34A-C35A	1.360(7)	1.394	N13B-N14B	1.333(5)	1.326
C35A-C36A	1.378(6)	1.393	N13B-Ni1B	1.793(4)	1.831
N2A-N3A	1.392(4)	1.375			

Angles	exp.	DFT	Angles	exp.	DFT
C15A-C1A-C18A	119.4(3)	119.1	C27A-N28A-C29A	115.9(4)	116.9
N2A-C1A-C15A	120.8(3)	121.4	N2A-Ni1A-N5A	83.42(14)	83.4
N2A-C1A-C18A	119.7(3)	119.3	N2A-Ni1A-N10A	173.19(13)	174.5
N3A-C4A-N5A	121.6(3)	121.2	N5A-Ni1A-N10A	102.37(14)	102.0
N3A-C4A-S1A	118.6(3)	119.5	N13A-Ni1A-N2A	91.98(13)	92.1
N5A-C4A-S1A	119.7(3)	119.2	N13A-Ni1A-N5A	171.17(14)	170.5
C24A-C7A-C8A	116.0(4)	116.1	N13A-Ni1A-N10A	82.74(13)	82.4
N6A-C7A-C8A	126.8(4)	126.7	C4A-S1A-C16A	100.1(2)	100.8
N6A-C7A-C24A	116.9(4)	117.3	C12A-S2A-C17A	100.82(18)	100.7
C7A-C8A-C8B	115.6(3)	115.4	C15B-C1B-C18B	125.1(7)	119.1
C9A-C8A-C7A	119.4(3)	109.4	N2B-C1B-C15B	120.5(4)	121.4
C9A-C8A-C8B	114.1(3)	113.5	N2B-C1B-C18B	114.4(7)	119.3

C25A-C9A-C8A	115.6(3)	117.9	N3B-C4B-S1B	118.2(3)	119.6
N10A-C9A-C8A	121.2(3)	119.7	N5B-C4B-N3B	122.0(4)	121.2
N10A-C9A-C25A	123.1(3)	122.3	N5B-C4B-S1B	119.7(4)	119.2
N11A-C12A-N13A	119.9(3)	119.9	C24B-C7B-C8B	115.0(4)	116.1
N11A-C12A-S2A	121.8(3)	121.2	N6B-C7B-C8B	126.9(4)	126.7
N13A-C12A-S2A	118.4(3)	118.9	N6B-C7B-C24B	118.2(4)	117.2
C1A-C15A-C31A	120.0(3)	120.5	C7B-C8B-C8A	109.3(3)	115.4
N14A-C15A-C1A	126.0(3)	125.8	C9B-C8B-C8A	114.3(3)	113.5
N14A-C15A-C31A	114.0(3)	113.7	C9B-C8B-C7B	115.2(3)	109.4
C19A-C18A-C1A	122.7(3)	120.2	C25B-C9B-C8B	115.4(4)	118.0
C23A-C18A-C1A	119.0(3)	120.6	N10B-C9B-C8B	121.4(4)	119.8
C23A-C18A-C19A	118.2(3)	119.2	N10B-C9B-C25B	123.1(4)	122.2
C20A-C19A-C18A	120.0(4)	120.4	N11B-C12B-N13B	118.8(4)	119.9
C21A-C20A-C19A	120.8(3)	120.2	N11B-C12B-S2B	121.5(3)	121.1
C22A-C21A-C20A	119.7(4)	119.7	N13B-C12B-S2B	119.7(3)	118.9
C21A-C22A-C23A	120.3(4)	120.2	C26B-C25B-C9B	122.4(3)	122.2
C22A-C23A-C18A	121.0(3)	120.4	C26B-C25B-C30B	117.8(4)	117.4
C26A-C25A-C9A	122.5(4)	120.0	C30B-C25B-C9B	119.5(4)	120.3
C30A-C25A-C9A	120.1(4)	120.5	C27B-C26B-C25B	119.1(4)	119.0
C30A-C25A-C26A	117.2(4)	117.6	N28B-C27B-C26B	123.9(4)	123.8
C27A-C26A-C25A	119.5(4)	119.1	N28B-C29B-C30B	123.0(4)	123.8
N28A-C27A-C26A	124.5(5)	123.8	C29B-C30B-C25B	119.0(4)	119.1
N28A-C29A-C30A	124.4(4)	123.9	C1B-N2B-N3B	115.8(3)	117.7
C25A-C30A-C29A	114.1(3)	119.0	C1B-N2B-Ni1B	128.5(3)	127.0
C32A-C31A-C15A	115.6(3)	121.4	N3B-N2B-Ni1B	115.6(3)	115.3
C32A-C31A-C36A	121.2(3)	118.6	C4B-N3B-N2B	108.0(3)	110.2
C36A-C31A-C15A	123.1(3)	119.9	C4B-N5B-N6B	114.8(4)	113.3
C31A-C32A-C33A	119.9(3)	120.7	C4B-N5B-Ni1B	110.9(3)	109.0
C34A-C33A-C32A	121.8(3)	120.3	N6B-N5B-Ni1B	131.8(3)	133.8
C33A-C34A-C35A	119.8(4)	119.6	C7B-N6B-N5B	121.6(3)	121.6

C34A-C35A-C36A	120.5(5)	120.2	C9B-N10B-N11B	113.8(3)	116.5
C35A-C36A-C31A	120.6(4)	120.7	C9B-N10B-Ni1B	131.7(3)	130.3
C1A-N2A-N3A	115.4(3)	117.8	N11B-N10B-Ni1B	114.2(2)	113.0
C1A-N2A-Ni1A	128.2(2)	127.0	C12B-N11B-N10B	108.5(3)	109.9
N3A-N2A-Ni1A	116.0(2)	115.3	C12B-N13B-Ni1B	114.0(3)	112.2
C4A-N3A-N2A	108.9(3)	110.2	N14B-N13B-C12B	113.3(4)	116.6
C4A-N5A-N6A	113.0(3)	113.4	N14B-N13B-Ni1B	132.7(3)	131.3
C4A-N5A-Ni1A	109.7(2)	109.0	C15B-N14B-N13B	120.8(4)	120.8
N6A-N5A-Ni1A	134.3(3)	133.8	C27B-N28B-C29B	117.2(4)	116.9
C7A-N6A-N5A	119.1(3)	121.6	N2B-Ni1B-N5B	83.05(16)	83.4
C9A-N10A-N11A	114.1(3)	116.6	N2B-Ni1B-N10B	173.28(14)	174.5
C9A-N10A-Ni1A	130.9(3)	130.2	N5B-Ni1B-N10B	103.16(15)	101.9
N11A-N10A-Ni1A	114.5(2)	112.8	N13B-Ni1B-N2B	91.32(16)	92.1
C12A-N11A-N10A	108.2(3)	109.9	N13B-Ni1B-N5B	171.65(14)	170.3
C12A-N13A-Ni1A	113.6(2)	112.1	N13B-Ni1B-N10B	82.78(15)	82.4
N14A-N13A-C12A	113.7(3)	116.6	C4B-S1B-C16B	101.0(3)	101.0
N14A-N13A-Ni1A	132.2(2)	131.3	C12B-S2B-C17B	100.9(2)	100.6
C15A-N14A-N13A	119.8(3)	120.8			

Compound **6a**

Distances	exp.	DFT	Distances	exp.	DFT
Ni1-N13	1.818(4)	1.831	C15-C1	1.461(8)	1.459
Ni1-N2	1.848(5)	1.864	C15-C31	1.488(8)	1.496
Ni1-N10	1.882(5)	1.912	C8-C7	1.521(8)	1.530
Ni1-N5	1.884(4)	1.894	C8-C8[1]	1.570(11)	1.574
S2-C12	1.733(6)	1.765	N11-C12	1.302(8)	1.299
S2-C17	1.797(7)	1.826	C1-C18	1.503(9)	1.496
S1-C4	1.759(5)	1.774	N6-C7	1.288(8)	1.281
S1-C16	1.793(7)	1.827	C18-C19	1.384(9)	1.398
N5-C4	1.297(8)	1.356	C18-C23	1.392(9)	1.399

N5-N6	1.400(7)	1.372	C22-C21	1.320(10)	1.396
N10-C9	1.299(8)	1.293	C22-C23	1.410(9)	1.392
N10-N11	1.431(6)	1.406	C34-C35	1.380(10)	1.394
N3-C4	1.326(8)	1.312	C34-C33	1.383(10)	1.394
N3-N2	1.378(6)	1.376	C31-C32	1.395(9)	1.401
N13-N14	1.328(7)	1.323	C31-C36	1.399(9)	1.401
N13-C12	1.385(8)	1.377	C24-C7	1.505(8)	1.505
N14-C15	1.317(8)	1.310	C33-C32	1.390(9)	1.393
N2-C1	1.321(8)	1.319	C19-C20	1.381(9)	1.394
C9-C25	1.493(8)	1.498	C36-C35	1.406(9)	1.393
C9-C8	1.512(8)	1.519	C21-C20	1.422(11)	1.393

Angles	exp.	DFT	Angles	exp.	DFT
N13-Ni1-N2	91.3(2)	92.1	C9-C8-C7	117.2(5)	113.2
N13-Ni1-N10	83.2(2)	82.6	C9-C8-C8[1]	110.2(5)	112.6
N2-Ni1-N10	174.1(2)	174.7	C7-C8-C8[1]	111.3(6)	113.1
N13-Ni1-N5	172.6(2)	170.1	C12-N11-N10	108.5(5)	109.9
N2-Ni1-N5	83.0(2)	83.3	N11-C12-N13	120.0(5)	120.0
N10-Ni1-N5	102.7(2)	102.0	N11-C12-S2	122.2(5)	121.4
C12-S2-C17	98.9(3)	100.4	N13-C12-S2	117.8(4)	118.6
C4-S1-C16	101.1(3)	100.9	N2-C1-C15	121.9(6)	121.4
C4-N5-N6	113.2(4)	113.3	N2-C1-C18	118.0(5)	119.2
C4-N5-Ni1	110.4(4)	109.1	C15-C1-C18	120.1(5)	119.2
N6-N5-Ni1	135.3(4)	134.4	C7-N6-N5	122.2(5)	121.4
C9-N10-N11	112.7(5)	115.7	C19-C18-C23	119.2(6)	119.2
C9-N10-Ni1	133.1(4)	131.2	C19-C18-C1	122.2(6)	120.2
N11-N10-Ni1	114.2(4)	113.1	C23-C18-C1	118.6(6)	120.7
C4-N3-N2	108.8(5)	110.2	C21-C22-C23	121.1(7)	120.2
N14-N13-C12	114.6(4)	116.4	C35-C34-C33	120.8(6)	119.5
N14-N13-Ni1	132.7(4)	131.4	C18-C23-C22	119.8(6)	120.4

C12-N13-Ni1	112.7(4)	112.2	C32-C31-C36	117.8(6)	118.5
C15-N14-N13	121.1(5)	121.0	C32-C31-C15	124.3(6)	121.6
C1-N2-N3	116.2(5)	117.4	C36-C31-C15	117.7(6)	119.8
C1-N2-Ni1	128.2(4)	127.2	N6-C7-C24	117.1(5)	117.2
N3-N2-Ni1	115.4(4)	115.3	N6-C7-C8	127.0(5)	127.0
N10-C9-C25	122.4(5)	122.9	C24-C7-C8	115.7(5)	115.8
N10-C9-C8	120.4(5)	120.4	C34-C33-C32	119.7(6)	120.3
C25-C9-C8	116.8(5)	116.7	C33-C32-C31	121.4(6)	120.7
N5-C4-N3	122.2(5)	121.4	C20-C19-C18	120.1(6)	120.4
N5-C4-S1	119.5(5)	119.1	C31-C36-C35	121.2(6)	120.8
N3-C4-S1	118.3(5)	119.5	C34-C35-C36	119.1(6)	120.2
N14-C15-C1	124.1(6)	125.8	C22-C21-C20	119.7(7)	120.2
N14-C15-C31	112.3(5)	113.6	C19-C20-C21	120.1(7)	120.2
C1-C15-C31	123.6(6)	120.6			

Symmetry code: [1] $1-x$, $-y$, $2-z$.

Table S2. Deviations (Å) from the mean least-squares plane in the seven-membered chelate ring(s).

Atom	4a	4s		5s		6a
		Part A	Part B	Part A	Part B	
Ni1*	0.075	–0.031	–0.028	–0.023	0.019	0.044
N5*	0.094	–0.182	–0.181	–0.177	0.172	0.108
N6*	–0.200	0.203	0.191	0.199	–0.191	–0.176
C7*	0.113	–0.041	–0.030	–0.044	0.039	0.082
C9*	0.083	–0.178	–0.184	–0.158	0.157	0.083
N10*	–0.165	0.228	0.231	0.204	–0.197	–0.141
C8	0.854(5)	0.877(2)	–0.856(2)	–0.846(6)	–0.856(6)	0.807(7)
RMS deviation of fitted atoms	0.130	0.164	0.162	0.153	0.148	0.114

*indicates atom used to define plane

IR spectroscopy

Most characteristic bands (cm^{-1}) for **4a**: 3053w, 2920m, 1597w, 1576w, 1529w, 1489vs, 1462s, 1441s, 1399vs, 1338m, 1319m, 1300vs, 1212vs, 1137s, 1074s, 941vs, 758s, 722m, 707m, 692vs, 592s, 565s and **4s**: 3056m, 3024m, 2924m, 1588m, 1573w, 1527m, 1486vs, 1456s, 1441s, 1399s, 1336s, 1325s, 1298vs, 1247s, 1213vs, 1187m, 1174s, 1140s, 940vs, 916s, 759s, 732s, 693vs, 672s, 592s, 568s.

Most characteristic bands (cm^{-1}) for **5s**: 3052w, 3021w 2997w, 2924m, 1585m, 1541m, 1482vs, 1442s, 1405s, 1321s, 1296vs, 1250m, 1209vs, 1137s, 1071s, 1026s, 1003s, 938vs, 918vs, 702vs, 675s, 622s, 591s, 564s, 517m, 480m.

Most characteristic bands (cm^{-1}) for **6s**: 3058w, 3020w 2995w, 2926m, 1606m, 1530s, 1499s, 1491s, 1461s, 1444m, 1395s, 1301vs, 1257s, 1248s, 1207vs, 1131s, 1077m, 949vs, 910s, 754s, 730s, 694vs, 665s, 621s, 605s, 572s, 463m, 414m. for **6a**: 3057w, 3022w 2985w, 2923m, 1602m, 1529m, 1490vs, 1458s, 1444m, 1394s, 1298vs, 1248s, 1202vs, 1131s, 1078m, 949vs, 907s, 754s, 732s, 699vs, 666s, 621s, 606s, 566s, 416m.
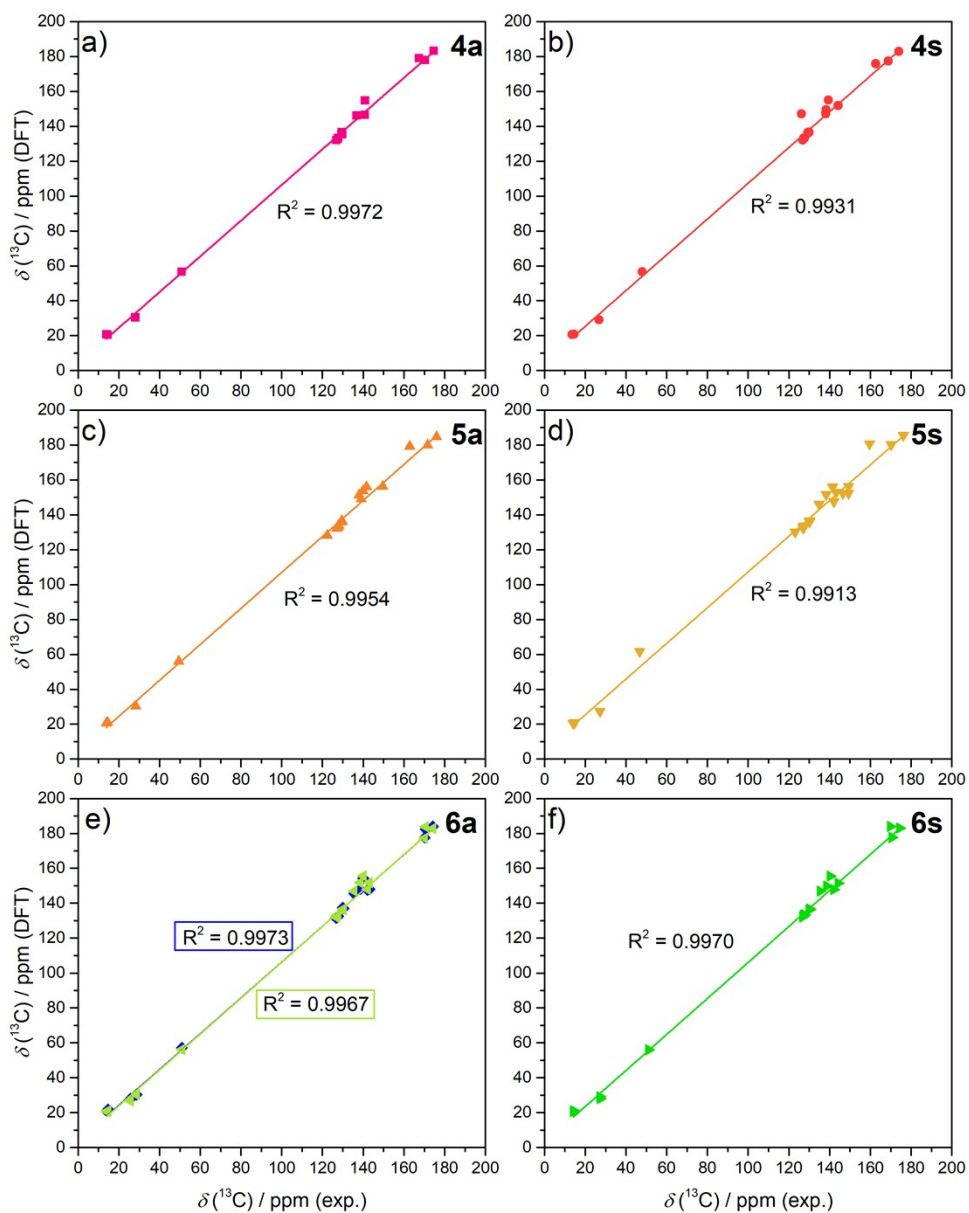
NMR spectroscopy
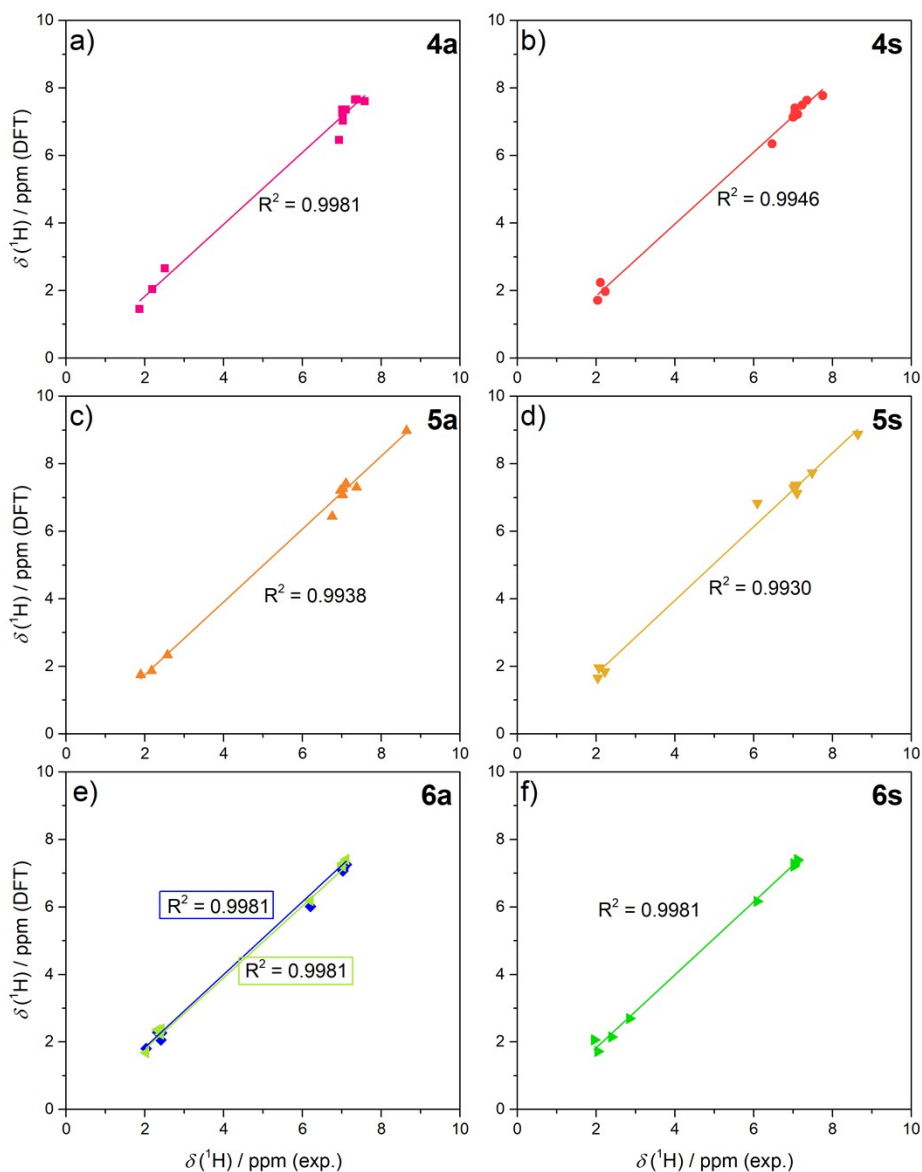
Figure S3. The correlation of the experimental and the B3LYP/6-311G* DFT predicted ^{1}H chemical shifts of a) **4a**, b) **4s**, c) **5a**, d) **5s**, e) **6a**, f) **6s**. DFT predicted shifts for magnetically equivalent CH_3, Ph and pyridyl protons were averaged, and the data are compared for the asymmetric part of the dimer (corresponding to the mononuclear Ni^{II} complex). e) DFT calculations were performed for two geometries of **6a**. Blue diamonds correspond to the **6a** optimized geometry based on SC-XRD structure; green triangles correspond to the **6a** optimized geometry with terminal phenyls rotation akin to the **4a** SC-XRD structure. The correlation coefficient R^2 from the linear regression analysis is displayed in each panel.

Figure S4. The correlation of the experimental and the B3LYP/6-311G* DFT predicted ^{13}C chemical shifts of a) **4a**, b) **4s**, c) **5a**, d) **5s**, e) **6a**, f) **6s**. DFT predicted shifts for magnetically equivalent CH_3 and Ph protons were averaged, and the data are compared for the asymmetric part of the dimer (corresponding to the mononuclear Ni^{II} complex). e) DFT calculations were performed for two geometries of **6a**. Blue diamonds correspond to the **6a** optimized geometry based on SC-XRD structure; green triangles correspond to the **6a** optimized geometry with terminal phenyls rotation akin to the **4a** SC-XRD structure. The correlation coefficient R^2 from the linear regression analysis is displayed in each panel.

Table S3. The assignment of the ^{1}H NMR chemical shifts, comparison of the experimental and the B3LYP/6-311G* DFT predicted NMR shifts.

	4a		4s		5a		5s		6a			6s	
						δ (^{1}H)/ ppm							
[a]	exp.	DFT	exp.	DFT	exp.	DFT	exp.	DFT	exp.	DFT[b]	DFT'[c]	exp.	DFT
H8	6.93	6.46	6.47	6.35	6.75	6.28	6.09	6.65	6.2	6.01	6.21	6.08	6.10
H16	1.87	1.45	2.04	1.71	1.89	1.71	2.04	1.62	2.03	1.80	1.64	2.04	1.68
H17	2.19	2.03	2.23	1.97	2.17	1.84	2.22	1.74	2.4	2.06	2.14	2.39	2.04
H19	7.03	7.03	7.00	7.13	7.02	7.03	7.1	7.09	7.02	7.19	7.12	7.02	7.13
H20	7.01	7.36	7.05	7.41	7.10	7.26	7.06	7.22	7.11	7.25	7.24	7.11	7.24
H21	7.10	7.36	7.12	7.22	7.10	7.25	7.09	7.22	7.11	7.25	7.24	7.11	7.23
H22	7.01	7.36	7.05	7.41	7.10	7.26	7.06	7.22	7.11	7.25	7.24	7.11	7.25
H23	7.03	7.03	7.00	7.13	7.02	7.03	7.1	7.09	7.02	7.19	7.12	7.02	7.24
H24	2.51	2.66	2.11	2.24	2.57	2.34	2.07	1.85	2.32	2.29	2.30	1.95	2.05
H25	–	–	–	–	–	–	–	–	2.42	2.26	2.37	2.85	2.64
H26	7.58	7.60	7.75	7.78	7.37	7.20	7.48	8.12	–	–	–	–	–
H27	7.34	7.65	7.35	7.64	8.64	8.92	8.64	8.87	–	–	–	–	–
H28	7.38	7.67	7.23	7.50	–	–	–	–	–	–	–	–	–
H29	7.34	7.65	7.35	7.64	8.64	8.92	8.64	8.87	–	–	–	–	–
H30	7.58	7.60	7.75	7.78	7.37	7.20	7.48	8.12	–	–	–	–	–
H32	7.03	7.25	7.05	7.19	6.96	7.14	7.02	7.25	7.02	7.07	7.18	7.02	7.17
H33	7.01	7.28	7.06	7.29	7.02	7.11	7.05	7.19	7.02	7.10	7.13	7.02	7.11
H34	7.01	7.26	7.05	7.28	7.02	7.11	7.05	7.19	7.02	7.13	7.12	7.02	7.11
H35	7.01	7.28	7.06	7.29	7.02	7.11	7.05	7.19	7.02	7.10	7.13	7.02	7.11
H36	7.03	7.25	7.05	7.19	6.96	7.14	7.02	7.25	7.02	7.07	7.18	7.02	7.17

[a] Atom numbering according to the SC-XRD structures in Figs. 1-4, S1 and Table S1. DFT predicted shifts for magnetically equivalent CH_3, Ph and pyridyl protons were averaged. [b] Chemical shifts for the DFT-optimized geometry based on the **6a** SC-XRD structure. [c] Chemical shifts for the DFT-optimized geometry of **6a** with terminal phenyls rotation akin to the **4a** SC-XRD structure.

Table S4. The assignment of the ^{13}C NMR chemical shifts, comparison of the experimental and the B3LYP/6-311G* DFT predicted NMR shifts.

	4a		4s		5a		5s		6a			6s	
						δ (^{13}C)/ ppm							
[a]	exp.[b]	DFT	exp.[b]	DFT	exp.	DFT	exp.	DFT	exp.	DFT[c]	DFT'[d]	exp.	DFT
C1	140.93	154.81	139.38	154.98	141.68	155.09	141.54	154.84	140.06	154.24	154.64	140.38	154.29
C4	170.37	177.94	168.90	177.38	171.66	180.40	170.23	181.42	170.18	177.59	178.55	170.73	179.55
C7	140.82	146.59	144.25	151.94	139.00	145.26	143.21	149.16	143.14	148.05	147.85	144.16	147.24
C8	50.88	56.65	48.07	56.56	49.44	56.84	46.74	58.83	50.98	57.12	56.87	51.03	55.60
C9	167.47	178.99	162.73	175.83	162.85	177.64	159.60	179.84	170.65	182.41	182.00	169.87	181.84
C12	174.67	183.34	174.00	182.92	176.07	185.38	176.24	185.56	174.22	184.08	183.74	174.47	183.94
C15	138.56	150.60	138.37	149.45	138.01	150.64	138.27	151.14	138.61	148.05	147.85	138.59	149.53
C16	14.57	20.49	14.54	20.82	14.47	21.34	14.79	21.17	14.73	21.75	21.20	14.79	21.22
C17	13.92	20.73	13.57	20.59	13.82	20.85	13.98	20.72	14.09	20.83	20.90	14.12	20.89
C18	*	146.68	*	147.02	*	145.57	134.89	145.88	135.57	145.54	146.55	135.48	146.58
C19	129.60	136.62	129.55	136.41	129.62	137.40	130.11	137.18	129.98	137.44	137.20	130.33	137.25
C20	127.60	133.07	127.30	133.17	127.46	132.32	127.01	132.26	127.31	131.90	132.22	127.06	132.19
C21	127.78	133.39	127.45	133.27	127.97	133.06	127.76	132.94	127.68	132.51	132.61	127.70	132.59
C22	127.60	133.07	127.30	133.17	127.46	132.32	127.01	132.26	127.31	131.90	132.22	127.06	132.19
C23	129.60	136.62	129.55	136.41	129.62	137.40	130.11	137.18	129.98	137.44	137.20	130.33	137.25
C24	28.11	30.46	26.79	29.04	28.33	30.17	27.20	27.52	28.69	30.32	30.31	27.18	29.29
C25	136.74	146.17	138.16	147.02	139.96	152.97	146.56	151.46	25.73	27.91	27.26	27.29	27.97
C26	129.86	135.33	129.45	136.42	122.37	128.08	123.06	129.86	–	–	–	–	–
C27	127.71	133.06	127.70	133.24	149.61	155.66	149.28	155.80	–	–	–	–	–
C28	129.75	135.46	129.90	136.57	–	–	–	–	–	–	–	–	–
C29	127.71	133.06	127.70	133.24	149.61	155.66	149.28	155.80	–	–	–	–	–
C30	129.86	135.33	129.45	136.42	122.37	128.08	123.06	129.86	–	–	–	–	–
C31	*	147.75	138.20	147.89	*	146.81	142.10	146.90	142.17	147.55	147.33	142.05	147.29
C32	129.30	135.92	129.30	136.00	129.62	135.85	130.11	135.96	130.34	136.97	136.15	129.96	136.07
C33	127.60	132.79	127.30	132.75	127.46	132.07	127.37	132.31	127.05	131.70	132.02	127.32	132.02
C34	126.90	132.02	126.90	131.98	126.97	131.47	126.97	131.85	126.69	131.48	131.24	126.73	131.31
C35	127.60	132.79	127.30	132.75	127.46	132.07	127.37	132.31	127.05	131.70	132.02	127.32	132.02
C36	129.30	135.92	129.30	136.00	129.62	135.85	130.11	135.96	130.34	136.97	136.15	129.96	136.07

[a] Atom numbering according to the SC-XRD structures in Figs. 1-4, S1 and Table S1. DFT predicted shifts for magnetically equivalent CH$_3$, Ph and pyridyl protons were averaged. [b] ^{13}C experimental chemical shifts are obtained from the correlation peaks in the 2D ^{1}H−^{13}C HSQC, HMBC spectra. [c] Shifts for the DFT-optimized geometry based on the **6a** SC-XRD structure. [d] Shifts for the DFT-optimized geometry of **6a** with terminal phenyls rotation akin to the **4a** SC-XRD structure. * labels atoms where the experimental assignments are missing due to the limited signal-to-noise ratio in the NMR spectra.

Kinetics of isomerization (epimerization)

The kinetics of the **5a→5s** and **6s→6a** epimerization reaction was followed by ^{1}H NMR in CD_3Cl. The molar ratio at the given reaction time point was evaluated via integration of the signals of (at least) five resonances for each isomer. The experimental kinetic traces were analyzed using two kinetic models (Figure S5):

1. First-order kinetics was assumed, and the experimental data were fitted with integrated rate law equation (example for the **5a→5s** reaction)

$$x(\mathbf{5a}) = e^{-kt}$$

    where x is the molar ratio of the decaying isomer, t is the reaction time, and k is the first order rate constant.

2. A model for reaction approaching equilibrium (e.g. $\mathbf{5a} \overset{k_f}{\underset{k_b}{\rightleftharpoons}} \mathbf{5s}$) was employed by fitting the data with integrated rate law of the form

$$x(\mathbf{5a}) = x_0(\mathbf{5a}) - \frac{k_f x_0(\mathbf{5a}) - k_b\left(1 - x_0(\mathbf{5a})\right)}{k_f + k_b}\left(1 - e^{-(k_f + k_b)t}\right), \quad K = \frac{k_f}{k_b}$$

    where x is the molar ratio of the decaying isomer, the x_0 molar ratio in the initial solution, t is the reaction time and k_f is the first-order rate constant for the forward reaction, k_b the first order rate constant for the backward reaction, and K is the equilibrium constant. According to the recommendation in A. Genaev, et al., *Org. Biomol. Chem.* 2019, 17, 3781-3789, k_f and K were optimized as independent parameters in the fit.

The rate constants and the K values obtained are summarized in Table S5.

Note that, since we haven't followed the **5** epimerization up to the point where equilibrium could have been reached, the estimated K(s) might be inaccurate. Nevertheless, the relatively invariable value of $K \approx 9$ estimated by the equilibrium model fit, at all investigated temperatures, is consistent with the **5s/5a** molar ratio of 92/8 found in an aged reaction mixture sample.

The activation parameters of epimerization **5** were extracted from the temperature dependence of k and k_f using Eyring,

$$\ln\left(\frac{k}{T}\right) = -\frac{\Delta H^{\ddagger}}{RT} + \frac{\Delta S^{\ddagger}}{R} + \ln\left(\frac{k_B}{h}\right)$$

and Arrhenius equations

$$\ln(k) = Ae^{-\frac{E_a}{RT}}$$

where, T stands for the temperature, R, k_B, h are the Gas, Boltzmann and Planck constants, respectively, and the $\Delta H^{\ddagger}$ and $\Delta S^{\ddagger}$ are the activation enthalpy and entropy, E_a is the activation energy and A the frequency factor. The activation parameters are displayed in the insets of Figure S5a,c.
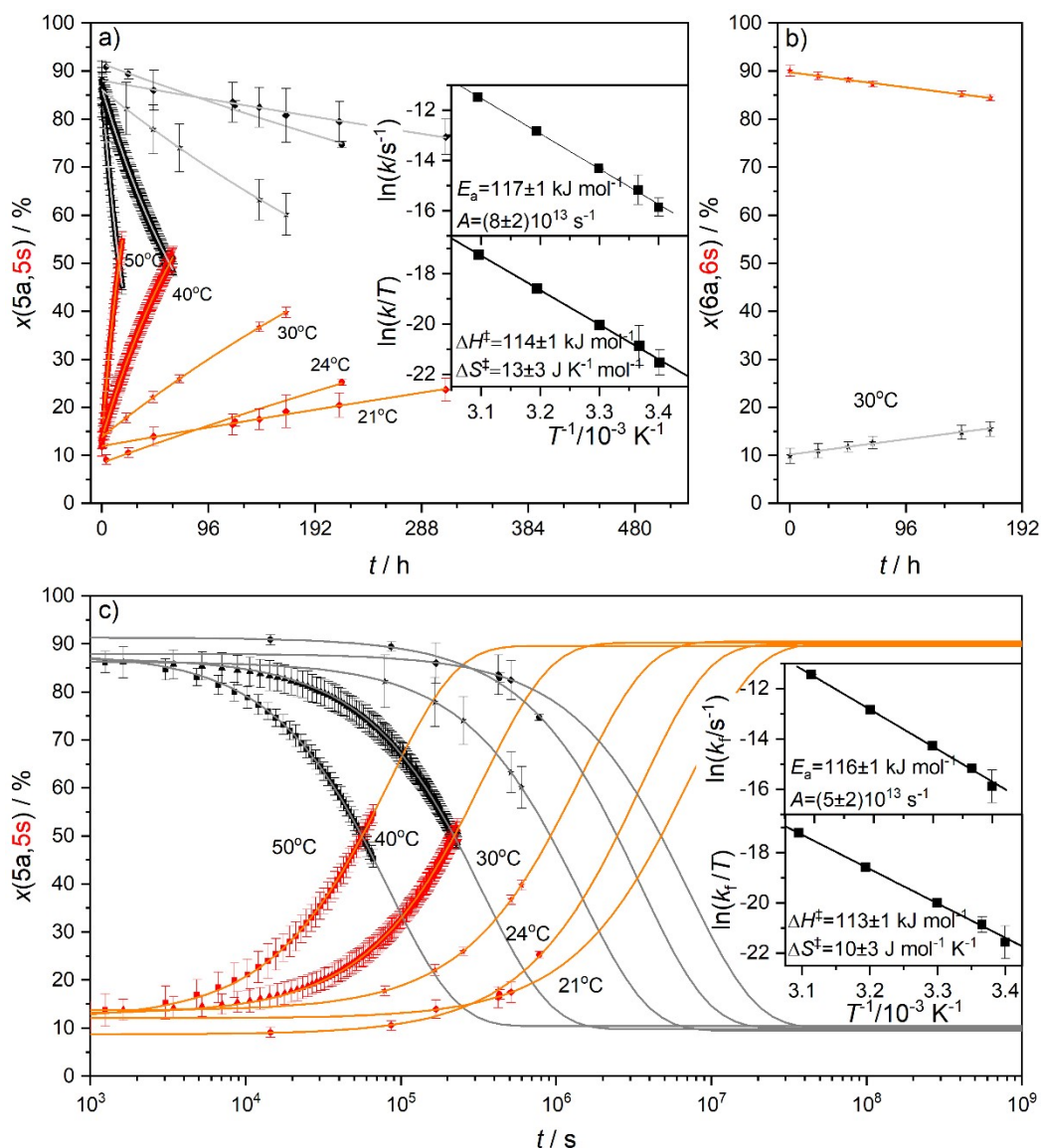

Figure S5. a) The kinetics of the **5a** to **5s** epimerization in CDCl$_3$ followed by ^{1}H NMR in the 21-50°C range. The circles correspond to the **5a** (black) and **5s** (red) molar ratio at a given reaction timepoint. Error bars reflect the deviation within two independent runs, and involve the integration errors of (at least) five resonances in the ^{1}H spectrum used for quantification of isomer concentration. Gray and orange lines represent the fits of the first order kinetic equation. Insets shows the analysis of rate constant temperature dependence using Arrhenius and Eyring equations, and the activation parameters. b) The kinetics of the **6s** to **6a** isomerization at 30°C. The rate of the conversion was found to be roughly five times slower than the isomerization of **5** (see Table S5). c) Evaluation of **5a** to **5s** epimerization kinetics with the model of

a reaction approaching equilibrium involving forward and backward reactions. Inset: Arrhenius and Eyring analysis of the temperature dependence of the forward reaction rate constant with corresponding activation parameters.

Table S5. The first-order rate constants of isomerization (epimerization) of **5a→5s** and **6s→6a** in CD_3Cl and the parameters the $\mathbf{5a} \underset{k_b}{\overset{k_f}{\rightleftharpoons}} \mathbf{5s}$ kinetic model

T /K	5a→5s k / $10^{-7}s^{-1}$	6s→6a	$\mathbf{5a} \underset{k_b}{\overset{k_f}{\rightleftharpoons}} \mathbf{5s}$ k_f / $10^{-7}s^{-1}$	K
294	1.30 ± 0.03	–	1.3 ± 0.8	9 ± 300
297	2.6 ± 0.1	–	2.58 ± 0.08	9 ± 24
303	6.03 ± 0.02	1.04 ± 0.04	6.30 ± 0.08	9.5 ± 3.1
313	26.7 ± 0.1	–	26.80 ± 0.08	9.2 ± 0.5
323	104 ± 1	–	107.5 ± 0.9	8.6 ± 1.2

Electrochemistry and spectroelectrochemistry
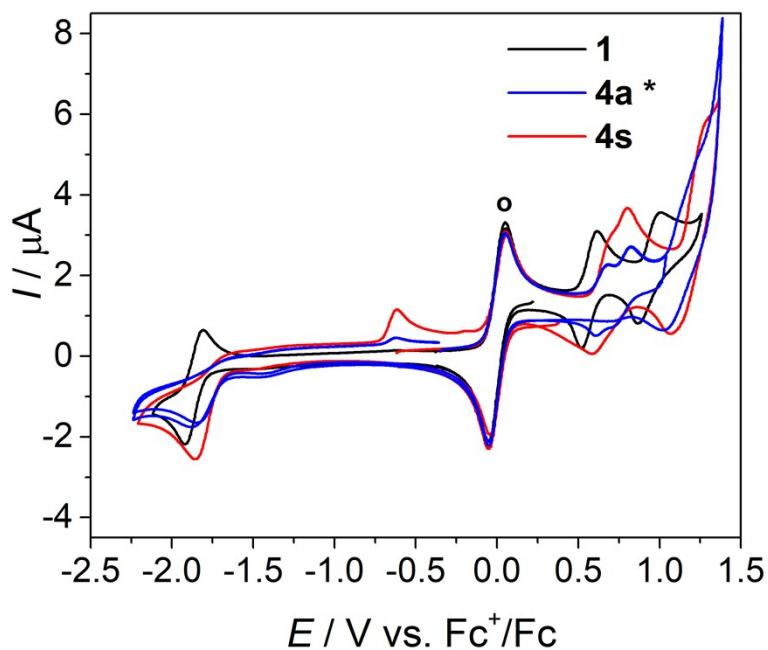
Figure S6. Cyclic voltammograms of 0.5 mM **1** (black trace), **4s** (red trace) in the presence of 0.5 mM **ferrocene** (o, Fc) (two scans, scan rate 200 mV s^{-1}) in CH_2Cl_2 /nBu$_4$NPF$_6$. CV of complex **4a,** with limited solubility in CH_2Cl_2 at saturated concentration about 0.2 mM (*), in the presence of 0.5 mM Fc, is shown as the blue trace. Note that due to the smaller size of the Fc molecule its diffusion coefficient is higher than for the mono or dinuclear Ni(II) macrocyclic complexes and results in larger peak currents at identical molar concentration.

Table S6. Electrochemical data for oxidation of selected mononuclear (**1**) and dinuclear (**4a**, **4s**) Ni(II) complexes derived from the square-wave voltammetry in $CH_2Cl_2/n\text{-}Bu_4NPF_6$ solutions using Pt working electrode. Anodic peak potentials (E_{pa}) for the first (ox1), second (ox2), third (ox3) and fourth (ox4) electron transfer respectively, are in volts vs Fc^+/Fc.

complex	E_{pa}^{ox1}		E_{pa}^{ox2}	
1	0.56		0.93	
	E_{pa}^{ox1}	E_{pa}^{ox2}	E_{pa}^{ox3}	E_{pa}^{ox4}
4a	0.63	0.76	1.17	1.25
4s	0.60	0.69	1.17	1.17
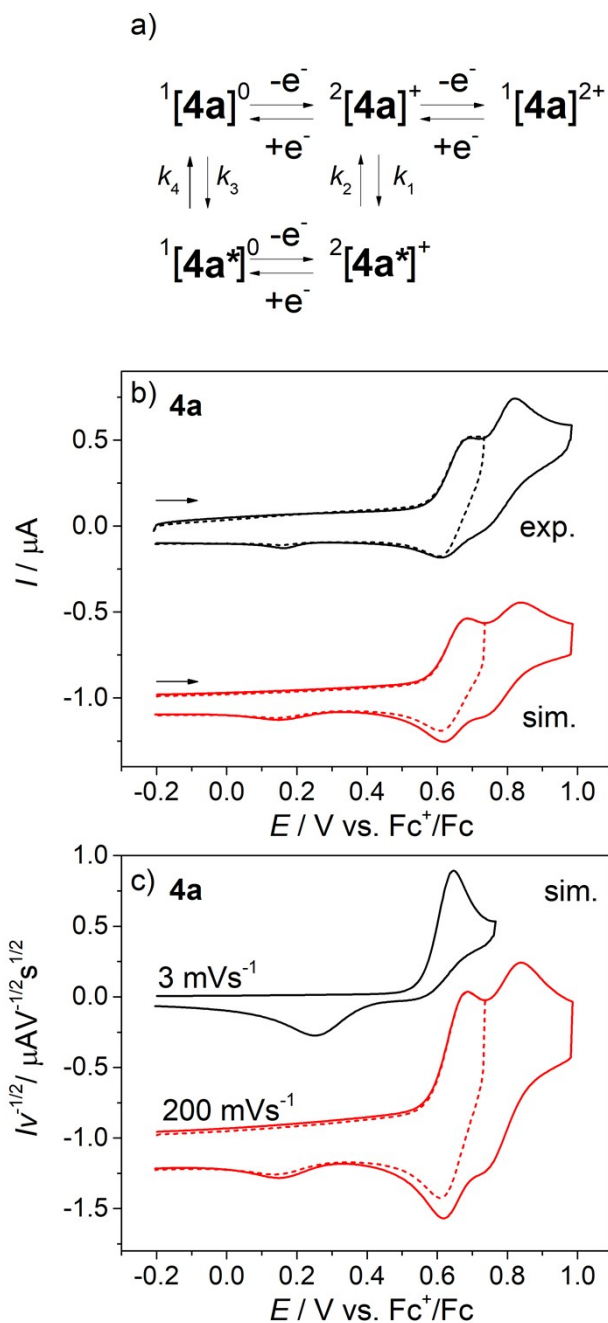
Figure S7. a) The mechanism proposed for the electro-chemical transformations of **4a** during the removal of the first two electrons; b) experimental CV (black) and digital simulations of CV (red - DigiElch Professional software from Gamry Instruments (USA), version Digielch8, was used for simulations) of **4a** at 200 mVs^{-1} according to the mechanism in a). Parameters: $E^o_{,ox1}$ = +0.65 V, $E^o_{,ox2}$ = +0.79 V for **4a** and $E^o_{,ox1}$ = +0.27 V for **4a*** vs Fc$^+$/Fc, k_s = 0.05 cm s^{-1}, α = 0.5, D = 10^{-5} cm^2 s^{-1}, k_1 = 0.6 s^{-1}, k_2 = 0.006 s^{-1}, k_3 = 1.6·10^{-8} s^{-1}, k_4 = 6·10^8 s^{-1}. c) digital simulations at 3 mVs^{-1} (black, for comparison with Fig. 10, inset) and 200 mVs^{-1} (red)
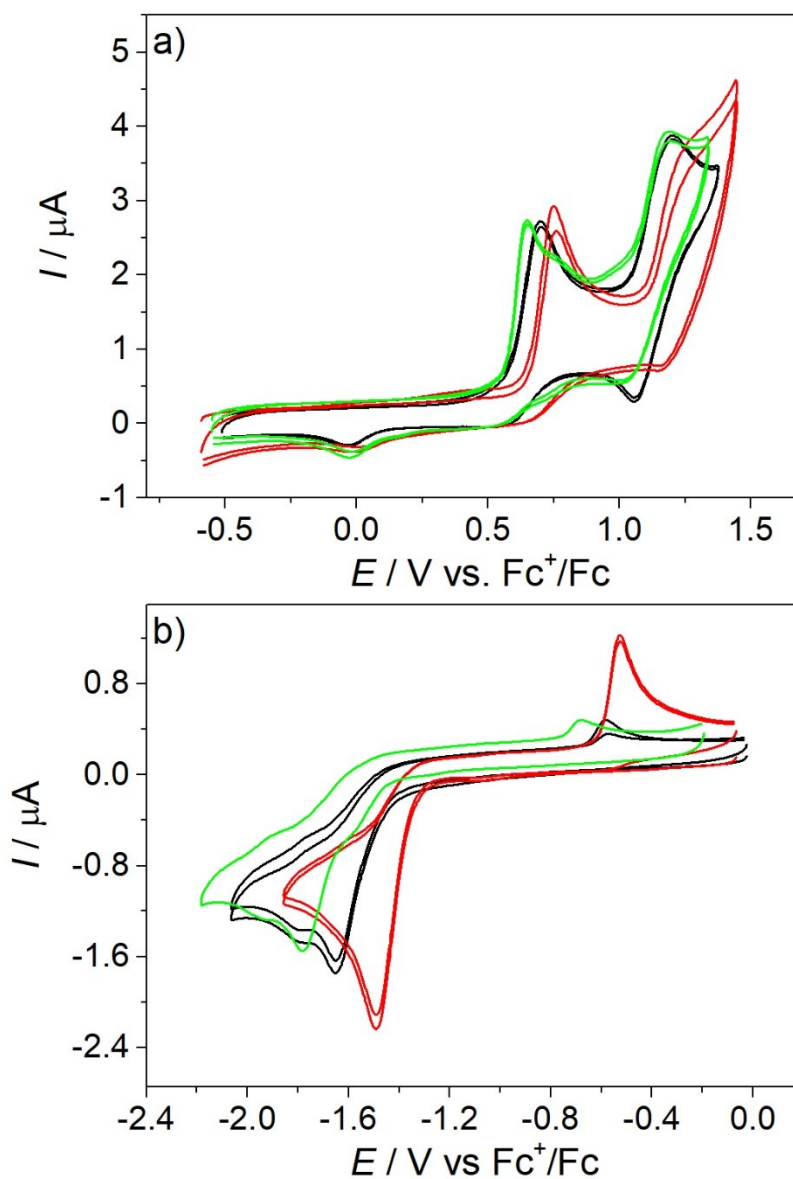
Figure S8. Cyclic voltammograms of **4s** (black traces), **5s** (red traces) and **6a** (green traces) in CH_2Cl_2-CH_3CN/nBu_4NPF_6 (two scans, scan rate 100 mV s^{-1}).
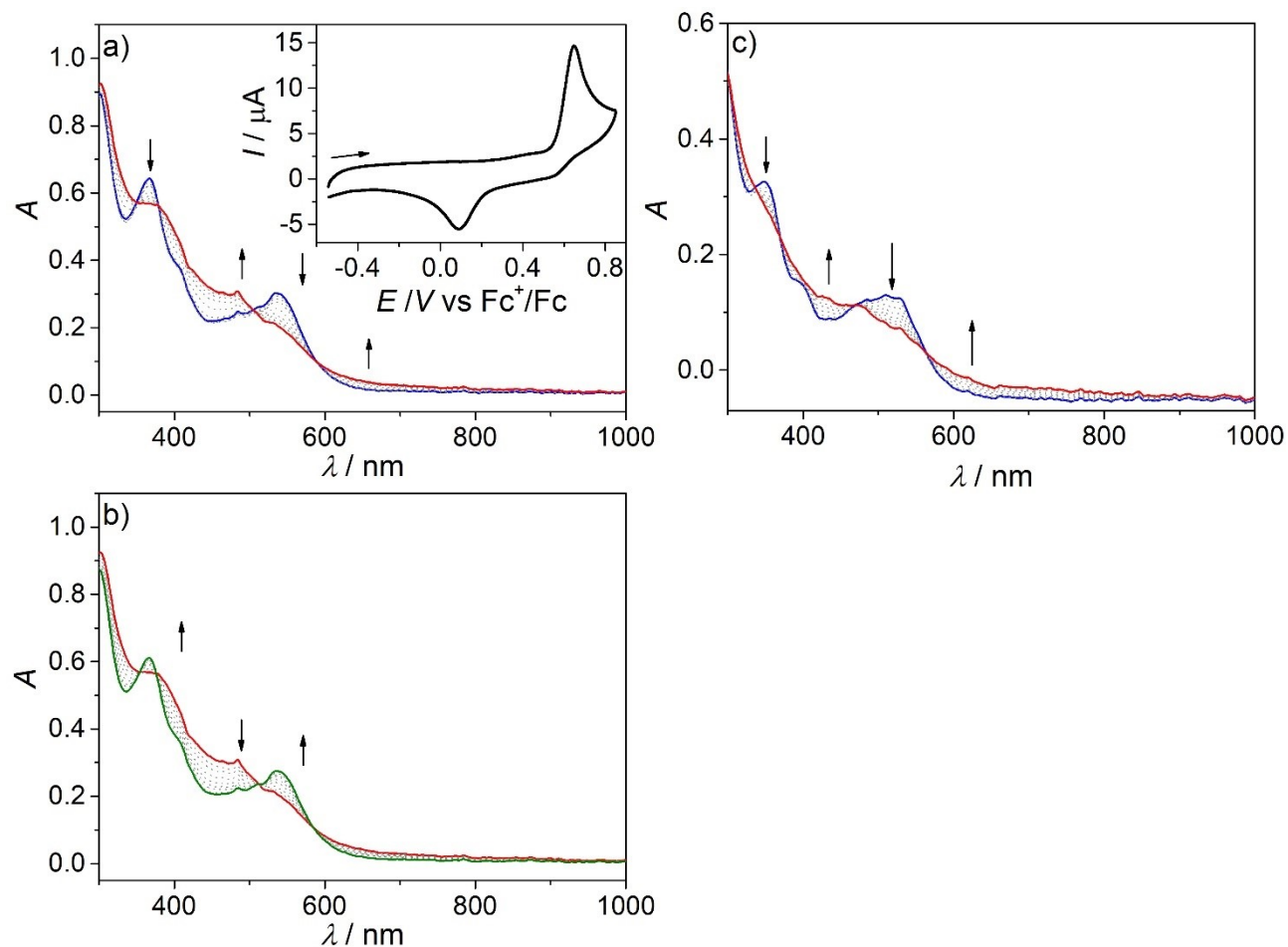
Figure S9. UV–vis–NIR spectra measured in the region of the first anodic 2-electron oxidation peak upon a) forward scan and b) during the backward scan of **4s** in CH_2Cl_2/CH_3CN $1:1/n$Bu$_4$NPF$_6$ under an argon atmosphere. Inset in a): in situ cyclic voltammogram (Pt-honeycomb working electrode, scan rate 10 mV s^{-1}). c) UV–vis–NIR spectra measured in the region of the first anodic double-peak upon forward scan of **6a** in CH_2Cl_2/CH_3CN $1:1/n$Bu$_4$NPF$_6$ under an argon atmosphere.
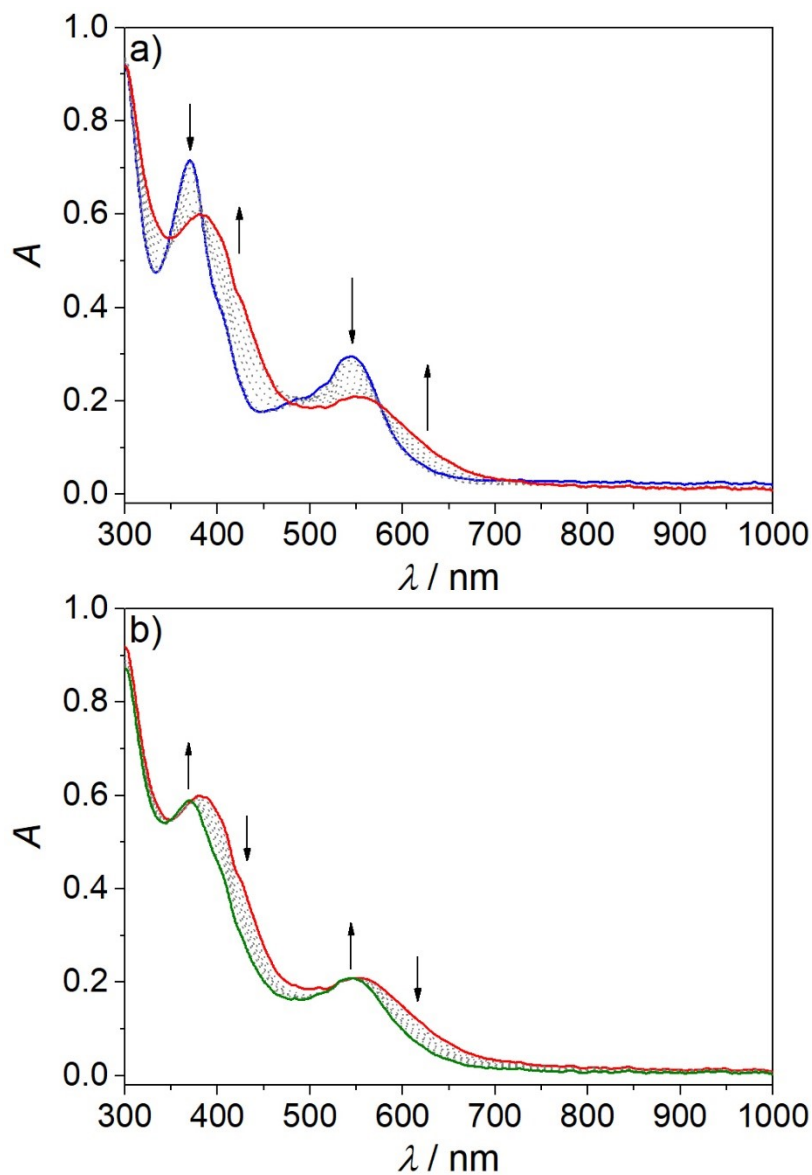
Figure S10. UV–vis–NIR spectra measured in the region of the first anodic peak upon (a) forward scan and (b) during the backward scan of **5s** in CH_2Cl_2/CH_3CN 1:1/nBu$_4$NPF$_6$ under an argon atmosphere (Pt-honeycomb working electrode, scan rate 10 mV s^{-1}).
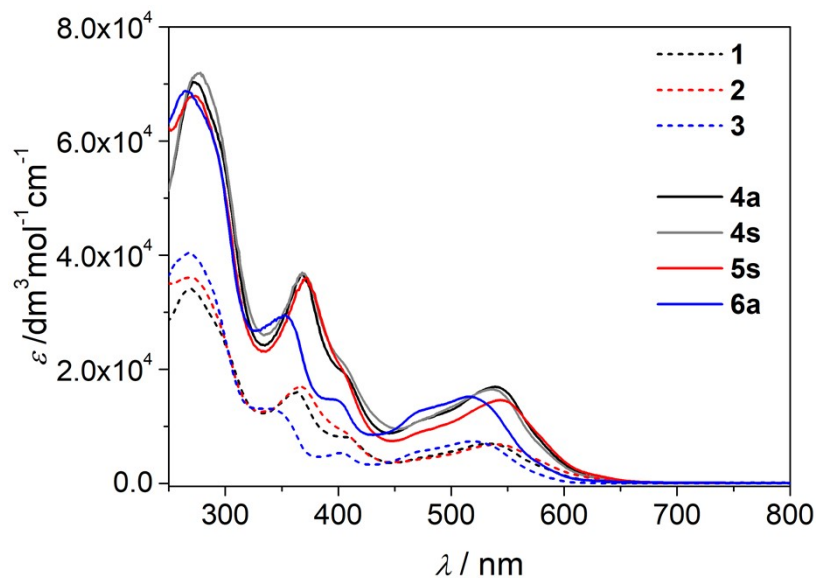
UV–vis–NIR spectroscopy

Figure S11. UV–vis spectra of (a) dimeric complexes **4a**, **4s**, **5s** and **6a** (solid lines) and (b) their corresponding monomeric precursors **1**, **2**, **3** in CH_2Cl_2.
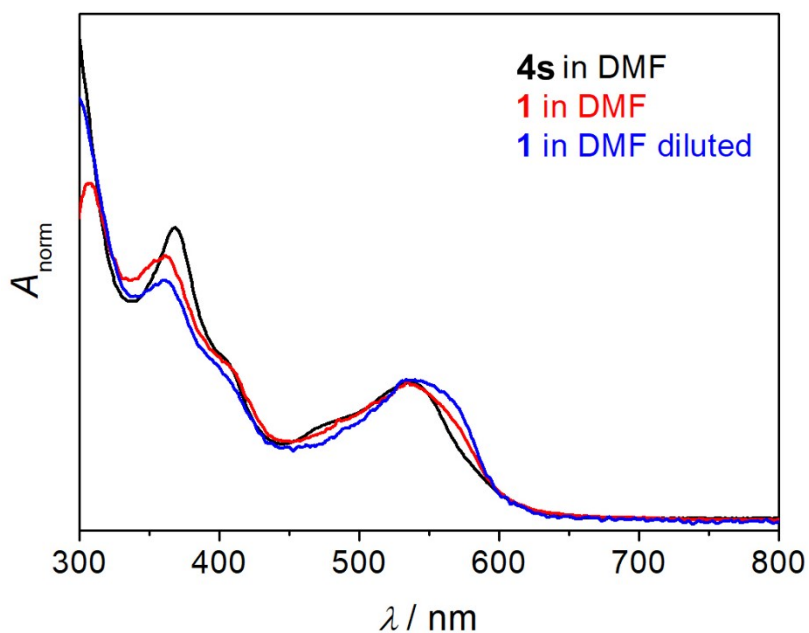

Figure S12. Normalized UV–vis spectra of dimeric complex **4s** (black trace) and of the corresponding monomer **1** (red trace) in DMF (blue trace – diluted monomer **1** in DMF). All the spectral traces are normalized to the absorption at 530 nm for comparison purposes.

DFT calculations

Considering the CV experiment as well as the *anti/syn* isomerization, it is worthwhile to provide some detail about the tautomeric and other forms of **4a** showing rich conformational variability of the compounds studied (both the initial neutral ones, as well as the follow up oxidation products). First of all, it is worth noting that, we have found a geometry with the Ni-C8-C8^i-Ni^i dihedral angle of 75.8° (denoted as ^{1}[**4a^{rot90}**]^0 see Figure S14a) and this geometry is 38.9 kJ·mol^{-1} above the experimental **4a** geometry with the 180° Ni-C8-C8^i-Ni^i dihedral angle. In the case of ^{1}[**4s^{rot90}**]^0, the difference to **4s** is 46.5 kJ·mol^{-1} and the Ni-C8-C8^i-Ni^i dihedral angle is 97.3°. A relaxed geometry with Ni-C8-C8^i-Ni^i dihedral angle frozen to 0° (denoted as ^{1}[**4a^{rot180}**]^0, see Figure S14b) is by 96.6 kJ·mol^{-1} above **4a** (this geometry contains one imaginary frequency). Another option for a structural change of **4** is a proton transfer from the bridge carbon atoms to the nitrogen atoms of the macrocycle resulting in the species denoted ^{1}[**4a$_{H4}$**]^0 (with the lowest energy structure being 123.6 kJ·mol^{-1} above the reference **4a** one, although there are 8 such isomers for both C-H groups). In the case of the oxidized form, the energy difference between ^{2}[**4a$_{H4}$**]$^+$ and ^{2}[**4a**]$^+$ is of 73.5 kJ·mol^{-1}. Interestingly, the structure with twofold intramolecular proton transfer ^{2}[**4a$_{2xH4}$**]$^+$ is shifted by 61.2 kJ·mol^{-1} from ^{2}[**4a**]$^+$. Furthermore, we could also find the ^{2}[**4a**]$^+$ structure with the Ni-C8-C8^i-Ni^i dihedral angle rotated to 81.5° and this geometry is by means of 33.4 kJ·mol^{-1} above ^{2}[**4a**]$^+$. In addition, several other structures have been found with respect to the structure variability and/or follow up products upon oxidation, one is related to bridging the two monomeric units via the C–N bond [**4a$_{CN}$**], a change of the orientation for the bridging C–C bond (*i.e.*, a change of orientation of the macrocycle and hydrogen on the particular sp^3 bridging carbon atom, a change similar to chair-boat conformations in cyclohexane) [**4a$_{CH-CH}$**] or a change of the macrocycle shape with respect to the nitrogen atom which is bonded to the central atom [**4a$_{1-1'}$**], see Figure S14 and Table S8. The [**4a$_{1-1'}$**] and [**4a$_{CH-CH}$**] structures are the closest in energy to the original [**4a**] structure when considering the neutral species (49.3 and 12.5 kJ·mol^{-1}, respectively) and oxidation (21.5 and 10.7 kJ·mol^{-1}, respectively). In the structures of ^{1}[**4a$_{CN}$**]^0 and ^{2}[**4a$_{CN}$**]$^+$, the energy difference to the **4a** references are 63.3 and 53.3 kJ·mol^{-1}, respectively. For completeness, neutral (^{1}[**4a$_h$**]$^-$ and ^{1}[**4s**]$^-$) and oxidized (^{2}[**4a$_h$**]^0, ^{2}[**4a$_{h'}$**]^0 or two ^{2}[**4a$_{hh'}$**]$^-$) structures with one (h and h') and both (hh') C–H protons removed from [**4a**] are also compiled in Table S8.

In an attempt to explain the *anti-syn* isomerization of **4a** to **4s**, the option of an intramolecular proton transfer ^{1}[**4a$_{H4}$**]^0 (see Supporting Information section DFT calculations) has been considered. A graphical representation of the energetics for several geometries of ^{1}[**4'$_{H4}$**]^0 is summarized in Figure S16. Figure S16 shows that after the ^{1}[**4a$_{H4}$**]^0 initiation, which can be based on a ^{1}[**4a^{rot90}**]^0 or ^{1}[**4a^{rot180}**]^0 intermediate,

several species exist which have a considerably perturbed geometry and can be considered as $^1[\mathbf{4'_{H4}}]^0$ *syn-anti* intermediates. Still, one can anticipate a 100 kJ·mol^{-1} barrier, that has to be overcome within the isomerization scheme itself: $^1[\mathbf{4a_{H4}}]^0 \rightarrow {}^1[\mathbf{4'_{H4}}]^0 \rightarrow {}^1[\mathbf{4s_{H4}}]^0$. However, the energy difference between $^1[\mathbf{4a}]^0$ and $^1[\mathbf{4a_{H4}}]^0$ structures (123.6 kJ·mol^{-1}) is already comparable to the experimentally estimated energy barrier (114±1 kJ·mol^{-1}). Hence, the $^1[\mathbf{4'_{H4}}]^0$ structure is above an intermediate geometry for the $^1[\mathbf{4a_{H4}}]^0$ to $^1[\mathbf{4a_{H4}}]^0$ isomerization. In addition, the deprotonation of **4a** can be considered as an alternative,[64] assuming that the flexibility of the deprotonated carbon atoms is nearly the same as for $^1[\mathbf{4'_{H4}}]^0$. Still, we do not target the way how the **4a** system deprotonates, except of assuming that the bridging sp^3 C8 carbons can be considered a weak acid. We also note that the addition of excess triethylamine, as an organic base, to the solution of **4a** in CH_2Cl_2 did not lead to the change of the UV–vis spectra of the complex. Further details of the isomerization mechanism are currently under investigation in our lab and will be reported in due course.

a)

ε / hartree

Δ=0.1062

b)

ε / hartree

LUMO +1

LUMO +2

LUMO

LUMO +1

HOMO

LUMO

HOMO -1

HOMO

HOMO -2

HOMO -1
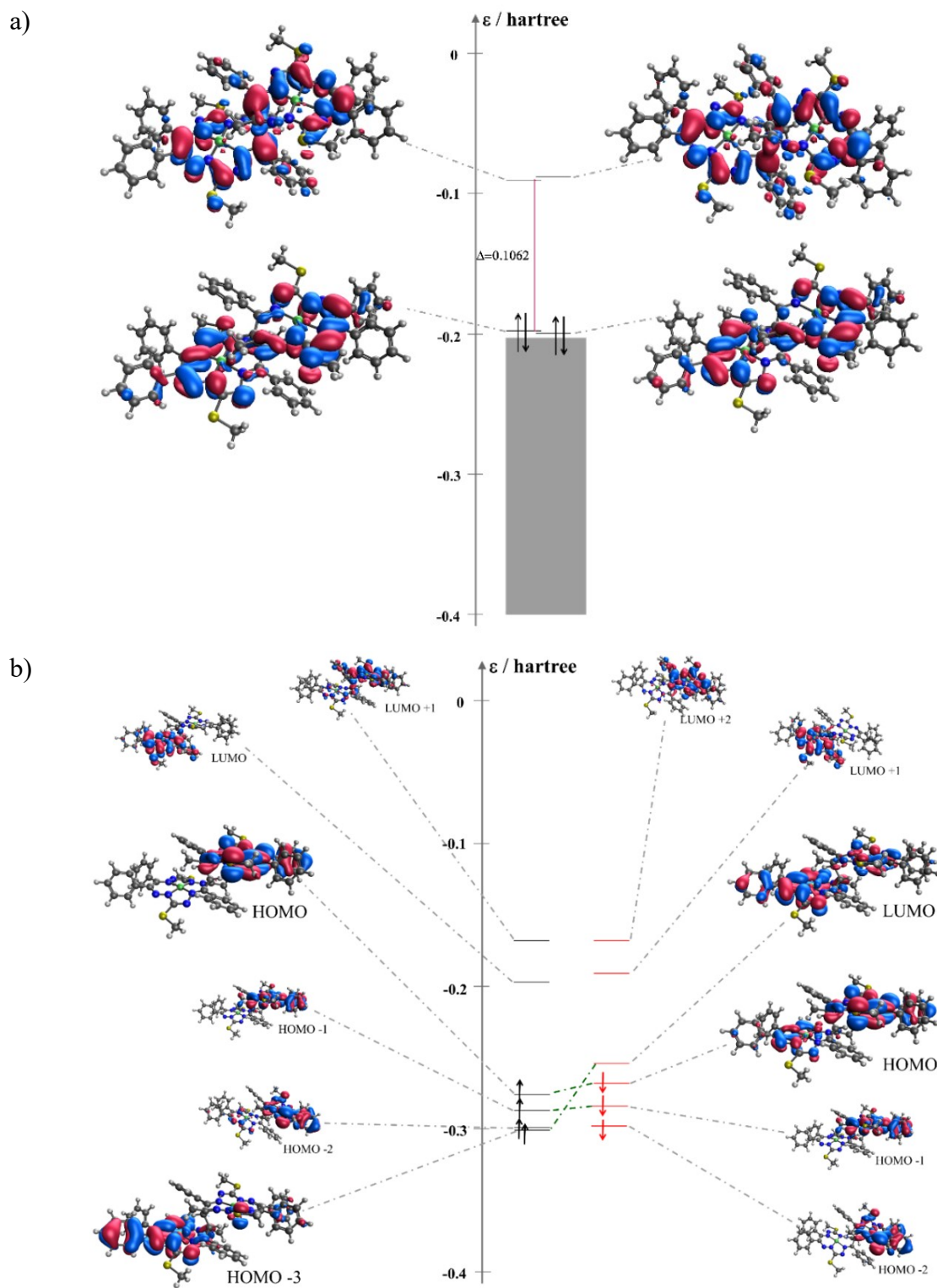
HOMO -3

HOMO -2

Figure S13. B3LYP/6-311G* frontier orbitals of a) ^{1}[**4a**]^0 and b) ^{2}[**4a**]$^+$ (isovalue 0.02 e.bohr$^{-3/2}$).
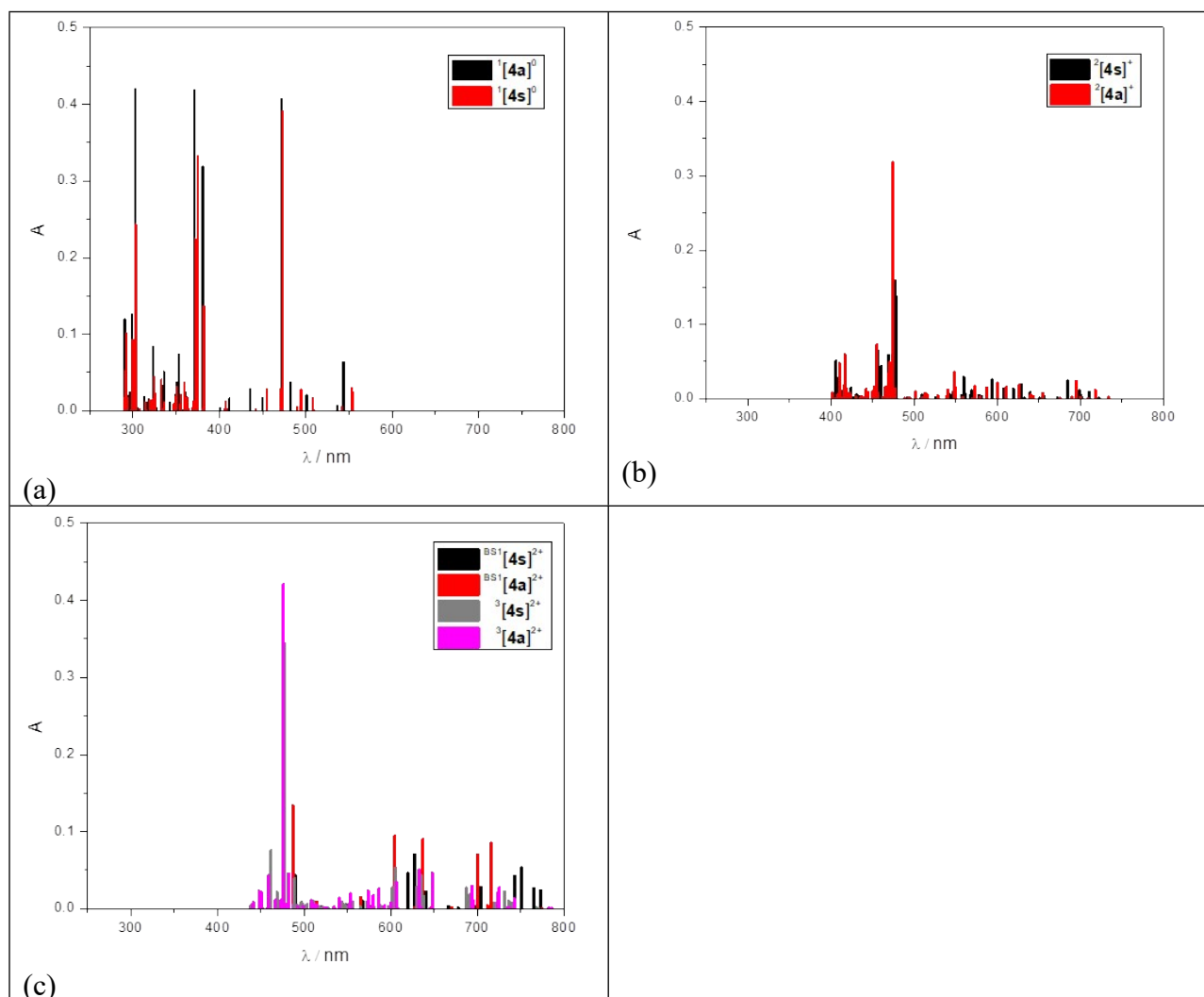
Figure S14. B3LYP/6-311G* TD transitions of (a) $^1[\mathbf{4s}]^0$ and $^1[\mathbf{4a}]^0$, (b) 1e-oxidized species of $^2[\mathbf{4s}]^+$ and $^2[\mathbf{4a}]^+$ and (c) 2e-oxidized species of $[\mathbf{4s}]^{2+}$ and $[\mathbf{4a}]^{2+}$.

(a) $^1[\mathbf{4a}^{rot90}]^0$

(b) $^1[\mathbf{4a}^{rot180}]^0$

(c) $^2[\mathbf{4a}_{1-1'}]^+$

(d) $^2[\mathbf{4a}_{CH-CH}]^+$

(e) $^2[\mathbf{4a}_{CN}]^+$

(f) $^2[\mathbf{4a}_{H4}]^+$
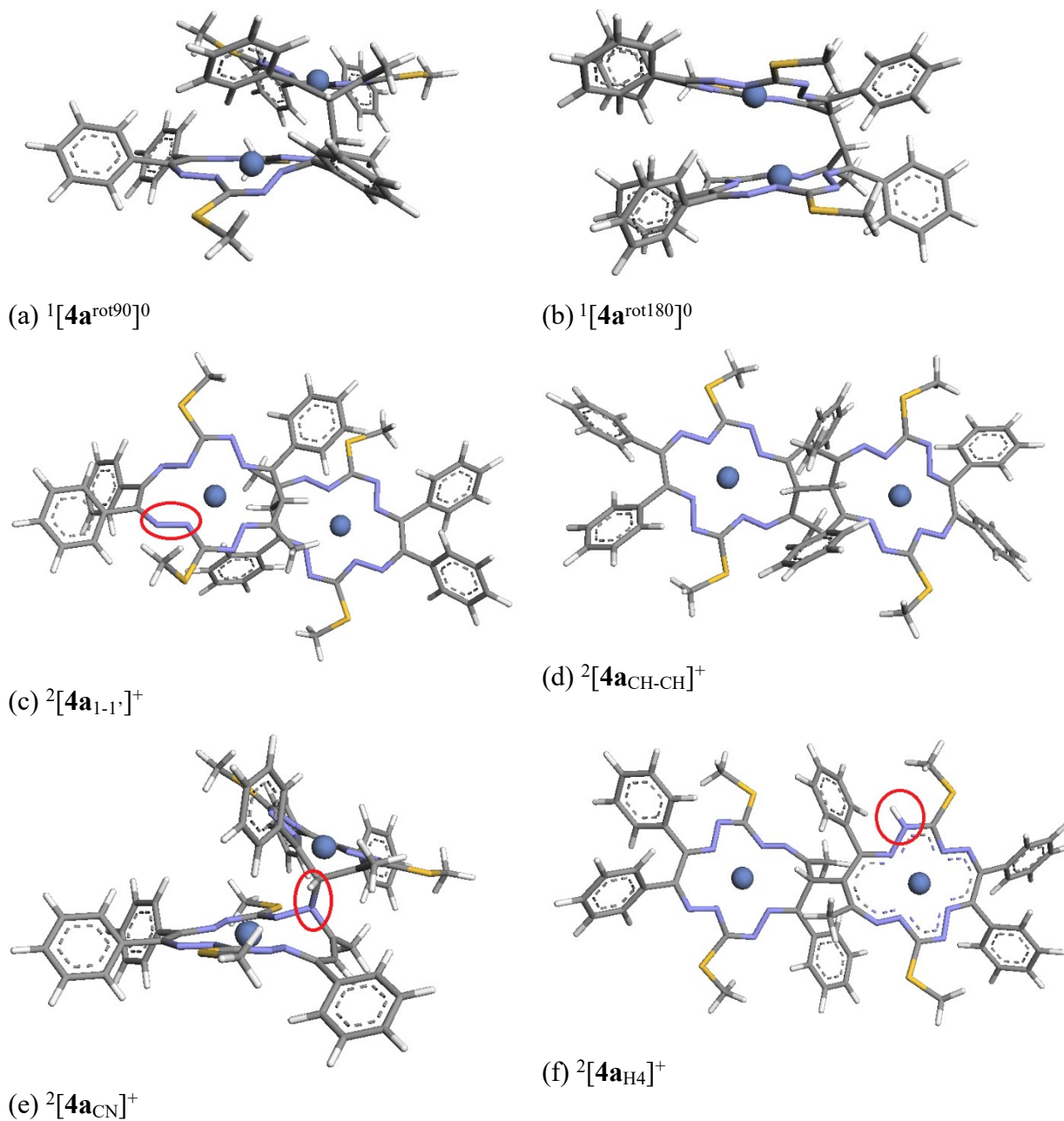
Figure S15. Optimized structure of $^1[\mathbf{4a}^{rot90}]^0$ with the 75.8° Ni-C8-C8^i-Ni^i dihedral angle (a), the relaxed structure $^1[\mathbf{4a}^{rot180}]^0$ with the 0° Ni-C8-C8^i-Ni^i dihedral angle frozen and of optimized structures of oxidized species $^2[\mathbf{4a}_{1-1'}]^+$ (c), $^2[\mathbf{4a}_{CH-CH}]^+$ (d), $^2[\mathbf{4a}_{CN}]^+$ (e), $^2[\mathbf{4a}_{CH-C,H4}]^+$ (f)

Figure S16. B3LYP/6-311G* energetics (free energies in kJ·mol^{-1}) of intermediate geometries of the isomerization for $^1[\mathbf{4_{H4}}]^0$ species (intramolecular proton transfer)

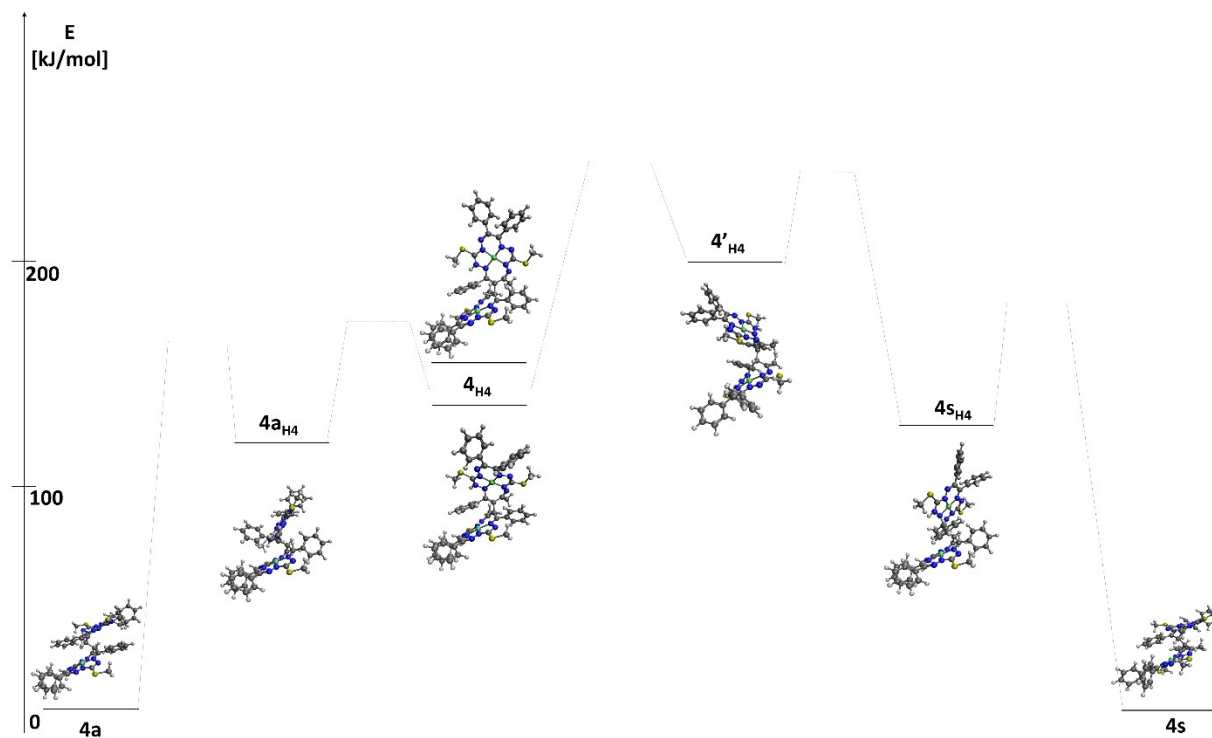**Table S7**. B3LYP/6-311G* energies of different isomers of [**4**], [**5**] and [**6**] and different spin and charged species of [**4**].

	E_{opt} [hartree]	S^2	q(Ni1)	q(Ni2)	spin(Ni1)	spin(Ni2)
^{1}[**4s**]^0	-7650.163002	0	1.027	1.026	0	0
^{3}[**4s**]^0	-7650.129146	2.007	1.270	1.027	1.607	0
^{2}[**4s**]$^+$	-7649.966307	0.773	1.023	1.050	0	0.008
^{1}[**4s**]$^{2+}$	-7649.740916	0	1.069	1.068	0	0
^{3}[**4s**]$^{2+}$	-7649.760646	2.044	1.068	1.060	0.009	0.008
^{BS}[**4s**]$^{2+}$	-7649.760651	1.044	1.068	1.060	0.009	-0.008
^{1}[**4a**]^0	-7650.161060	0	1.020	1.020	0	0
^{3}[**4a**]^0	-7650.085230	2.015	1.020	1.020	0.002	0.002
^{2}[**4a**]$^+$	-7649.964428	0.773	1.023	1.050	0.000	0.008
^{1}[**4a**]$^{2+}$	-7649.737013	0	1.055	1.057	0	0
^{3}[**4a**]$^{2+}$	-7649.758893	2.045	1.055	1.053	0.011	0.011
^{BS}[**4a**]$^{2+}$	-7649.758897	1.045	1.055	1.053	0.011	-0.010
^{2}[**4a**]$^-$	-7650.266813	0.769	1.015	0.997	0.001	-0.015
^{1}[**4a**]$^{2-}$	-7650.340318	0	0.991	0.992	0	0
^{3}[**4a**]$^{2-}$	-7650.354858	2.044	0.989	0.988	-0.007	-0.001
^{BS}[**4a**]$^{2-}$	-7650.354877	1.042	0.989	0.988	-0.008	-0.002
^{1}[**5s**]^0	-7682.247077	0	1.025	1.026	0	0
^{1}[**5a**]^0	-7682.245511	0	1.021	1.023	0	0
^{1}[**6s**]^0	-7266.627638	0	1.020	1.018	0	0
^{1}[**6a**]^0	-7266.628555	0	1.019	1.019	0	0

Table S8. B3LYP/6-311G* energies of chosen forms of [**4**] and [**4**]$^+$.

	E_{opt} [hartree]	S^2	q(Ni1)	q(Ni2)	spin(Ni1)	spin(Ni2)
$^1[\mathbf{4s}^{\mathbf{rot90}}]^0$	-7650.145281	0	1.026	1.026	0	0
$^1[\mathbf{4a}^{\mathbf{rot90}}]^0$	-7650.146255	0	1.032	1.015	0	0
$^1[\mathbf{4a}^{\mathbf{rot180}}]^{0,a}$	-7650.124257	0	1.006	1.010	0	0
$^1[\mathbf{4a}_{\mathbf{CH\text{-}CH}}]^0$	-7650.156308	0	1.015	1.015	0	0
$^1[\mathbf{4a}_{\mathbf{1\text{-}1'}}]^0$	-7650.142264	0	1.022	1.004	0	0
$^1[\mathbf{4a}_{\mathbf{CN}}]^0$	-7650.136945	0	1.035	1.016	0	0
$^1[\mathbf{4a}_{\mathbf{H4}}]^0$	-7650.113973	0	1.030	1.026	0	0
$^2[\mathbf{4a}^{\mathbf{rot90}}]^+$	-7649.951714	0.772	1.068	1.020	0.012	0.000
$^2[\mathbf{4a}^{\mathbf{rot180}}]^+$	-7649.931949	0.765	1.021	1.020	0.011	0.010
$^2[\mathbf{4a}_{\mathbf{CH\text{-}CH}}]^+$	-7649.960343	0.774	1.018	1.050	0	0.004
$^2[\mathbf{4a}_{\mathbf{1\text{-}1'}}]^+$	-7649.956253	0.770	1.024	1.058	0	0.070
$^2[\mathbf{4a}_{\mathbf{CN}}]^+$	-7649.944138	0.771	1.081	1.026	0.039	0.001
$^2[\mathbf{4a}_{\mathbf{H4}}]^+$	-7649.936417	0.777	1.052	1.037	0.022	0.012
$^2[\mathbf{4a}_{\mathbf{2xH4}}]^+$	-7649.941116	0.765	1.045	1.024	0.014	0.031
$^1[\mathbf{4s}_{\mathbf{h}}]^-$	-7649.649700	0	0.967	1.020	0	0
$^1[\mathbf{4a}_{\mathbf{h}}]^-$	-7649.649289	0	1.021	0.997	0	0
$^2[\mathbf{4a}_{\mathbf{h}}]^0$	-7649.505563	0.768	1.026	1.023	0.006	0.007
$^2[\mathbf{4a}_{\mathbf{h'}}]^0$	-7649.505577	0.770	1.024	1.026	0.007	0.006
$^2[\mathbf{4a}_{\mathbf{hh'}}]^-$	-7649.049240	0.760	0.996	0.995	-0.004	-0.002

^{a} relaxed geometry for the frozen Ni-C8-C8^i-Ni^i dihedral angle

Table S9. Crystal data and details of data collection for **4a**, **4s**, **5s** and **6a**.

Compound	4a	4s	5s	6a
empirical formula	$C_{56}H_{50}N_{16}Ni_{26}S_4$	$C_{58}H_{52}Ni_2Cl_6N_{16}S_4$	$C_{54}H_{48}Ni_2N_{18}S_4$	$C_{46}H_{646}Ni_2N_{16}S_4$
fw	1192.78	1431.51	1194.76	1068.65
space group	$P2_1/n$	$P\bar{1}$	$I4_1/a$	$P2_1/n$
a [Å]	10.5994(11)	11.30.32(11)	34.235(5)	10.6789(7)
b [Å]	14.0392(14)	15.7119(8)	34.235(5)	18.7474(13)
c [Å]	21.2185(17)	19.9582(12)	20.889(4)	11.7267(7)
α [°]		92.547(2)		
β [°]	100.972(4)	105.088(3)		91.7267(7)
γ [°]		108.429(3)		
V [Å³]	3099.7(5)	3110.2(4)	24483(9)	2346.6(3)
Z	2	2	16	2
λ [Å]	0.71073	0.71073	0.71073	0.71073
ρ_{calcd} [g cm⁻³]	1.278	1.529	1.297	1.512
crystal size [mm]	0.04 × 0.03 × 0.02	0.08 × 0.04 × 0.03	0.05× 0.04 × 0.04	0.09 × 0.08 × 0.04
T [K]	100(2)	100(2)	100(2)	100(2)
μ [mm⁻¹]	0.760	1.051	0.771	1.035
R_1[a]	0.0459	0.0426	0.0543	0.0766
wR_2[b]	0.1160	0.1057	0.1736	0.1803
GOF[c]	1.038	1.014	1.032	1.115

[a] $R_1 = \Sigma||F_o| - |F_c||/\Sigma|F_o|$. [b] $wR_2 = \{\Sigma[w(F_o^2 - F_c^2)^2]/\Sigma[w(F_o^2)^2]\}^{1/2}$. [c] GOF $= \{\Sigma[w(F_o^2 - F_c^2)^2]/(n - p)\}^{1/2}$, where n is the number of reflections and p is the total number of parameters refined.